CONTROL OF HYBRID DYNAMICS WITH APPLICATION TO A HOPPING ROBOT

By

Frank Benton Mathis

A DISSERTATION

Submitted to
Michigan State University
in partial fulfillment of the requirements
for the degree of

Mechanical Engineering - Doctor of Philosophy

2016

ABSTRACT

CONTROL OF HYBRID DYNAMICS WITH APPLICATION TO A HOPPING ROBOT

By

Frank Benton Mathis

Control of dynamic motion is an important subject of study in robotics as it is desirable for robots to have a specific motion pattern rather then moving to a set point. The motions of robots also involve changing dynamic behaviors due to interaction with the environment, such as during contact, and this leads to hybrid system dynamics. A popular example of a hybrid dynamical system is a legged robot; the hybrid dynamics is due to the periodic switching of swing and stance legs and impulsive dynamics due to ground contacts. Legged robots require control of a dynamic trajectory defined by the walking gait or running motion. For legged robots, the spring loaded inverted pendulum (SLIP) model is commonly used to describe the dynamic motion in a simplified manner. The SLIP model has also been used for control of hopping robots and a fundamental limitation of the model is that it fails to account for impact with the ground; this is due to its single degree-of-freedom in the vertical direction. We investigate the control of a hopping robot starting from a more general two-mass model and then expand the theory to planar multi-link robot systems. The investigation involves two ground contact models, rigid and elastic, for the objective of apex height control. In the rigid case, the ground is assumed to provide an impulsive force to the hopping robot resulting in an inelastic collision. A hybrid control strategy is designed to deal with the hybrid dynamical system: a continuous controller based on partial feedback linearization is used in conjunction with a discrete controller that updates a control parameter at each hop to achieve the control objective. In the elastic case, the ground acts as a massless spring, which

deflects as the robot exerts a force upon contact. In this case, we show that a continuous controller based on the backstepping algorithm can ensure asymptotic convergence to the desired apex height. Several robot configurations are considered, and for each configuration the complete hybrid dynamics is taken into account while designing the controller. The controllers compensate for the impulsive dynamics as well as higher order dynamics that are ignored in simplified models such as the SLIP model. Experimental validation of apex height control of a two-mass hopping robot on a rigid foundation is provided.

TABLE OF CONTENTS

LIST OF FIGURES

Chapter 1

Introduction

A hybrid dynamic system is one whose dynamics changes according to discrete events. Such systems are ubiquitous in robotics since a robot is frequently expected to interact with its environment causing either a discrete change in mass due to it picking up or dropping an object, or a change in kinematics due to contact with a surface such as the ground. Moreover, the dynamic motion of robots inspired by biological design, such as swimming with a tail or walking with legs, is not only hybrid in nature but also requires control to a periodic operating point. Here we will investigate the hopping motion of a robot which is inspired by running and waking in legged robotic systems.

The earliest work on hopping robots can be credited to Raibert [26], [14]. In his work, Raibert used a single mass on a hydraulic piston and experimentally demonstrated a hopping gait; the control design utilized a spring like motion in the piston and a stabilizing torque at the hip joint. Schwind and Koditchek [30] proposed a lossless model of Raibert's planar hopper for the purpose of controlling its forward velocity. A closed form of the return map of a hop was derived and a controller was proposed for improving upon the gait of Raibert's hopper. Saranli et al. [28] introduced the SLIP (spring loaded inverted pendulum) model of the hopper and argued its equivalence to the higher degree-of-freedom AKH (ankle-knee-hip) leg model. A deadbeat controller, which varied the spring parameters of the SLIP model at each hop, was designed to produce stable periodic motion. The spring loaded inverted pendulum (SLIP) model was later shown to be an accurate representation of running and

hopping in biological systems [5], [8].

Following the work by Schwind and Koditchek [30] and Saranli et al. [28], the SLIP model became very popular in the research community. Hyon used a combination of hydraulic actuators and springs to apply Raibert's control method to a kneed robot [16]. Kajita used a resolved momentum approach to control a legged robot to a desired trajectory [18]. Ghigliazza et al. [12], [11] and Holmes et al. [15] investigated passive stability of the SLIP model for various parameters. Poulakakis and Grizzle [24], [25] investigated the SLIP model with an asymmetric mass and compared its behavior with that of a three-link hopper. Altendorfer et al. [6], [7] studied the return map of the non-integrable SLIP dynamics and investigated the stability of the map. Seipel and Holmes [31], [32] investigated the stability of the SLIP model for a three-dimensional system. Hamed and Grizzle [13] later proposed a robust event-based control method to improve stability of the controlled legged system. Although the analysis of the SLIP model is useful and provides the basis for the design of effective controllers, it is incomplete since it does not account for the impulsive dynamics associated with foot-ground interaction.

The SLIP model is not capable of accounting for the impulsive forces that are generated at the time of impact with the ground. To account for these impulsive forces and model the dynamics of the hopper more accurately, it is necessary to model the leg as a mass rather than a massless spring. Saitou et al. [27] and Ishikawa et al. [17] proposed a two-mass system for a hopping robot in an effort to obtain a more accurate model of the robot in the flight phase. Saitou et al. [27] used optimal control methods to maximized the jumping height of the robot in the presence of control constraints. Ishikawa et al. [17] used a port-controlled Hamiltonian method to control the energy of the two mass system to a desired level to maintain a maximum jumping height. In both instances, the ground is modeled as

a spring and the impulsive effect of ground impact is neglected.

Here we investigate a class of hopping robots with two masses, three links, and four links. The control objective for each hopping robot is the achieve a desired maximum value of the center of mass during each hop, or apex height. All of which utilize a form a chaotic control strategies as the method for stabilizing the apex height. We begin in Chapter 2 with a two-mass hopping robot undergoing inelastic collision with a rigid ground at each hop. We use feedback linearization methods to stabilize the internal dynamics with different control parameters. The periodic nature and stability characteristics of the resulting hybrid dynamic system was analyzed [9] and "chaos control" [29] was used to discretely adjust a system parameter and converge the apex height to its desired value. Experimental results are presented in Chapter 2.6 using a voice coil actuator to prove the efficacy of the control method.

In Chapter 3, we extend the control method utilized on the two-mass hopping robot on an rigid ground to contol the apex height of a four-link hopping robot which undergoes inelastic collision with a rigid ground. Generalizing the control method from a two-mass robot to a four-link robot shows the applicability of the control to a more humanoid inspired system, as well as provides insights as to the method of extending the control method to system with higher degrees of freedom. The control method for the four-link hopping robot, as with the two mass hopping robot, utilizes feedback linearization to stabilize the system, and then a discrete change in a parameter each hop to converge the apex height to a chosen desired value.

Chapter 4 investigates the issues of applying the control strategy, which was developed for hopping on a rigid ground, to the case with the elastic ground. We then develop a new control method for controlling the two-mass hopper on the elastic ground. The control

method utilizes a continuous control method based on backsetpping. The backstepping method controls the energy of the system to a desired level while simultaneously controlling the distance between the two masses to a constant value. The hybrid dynamics are then stabilized utilizing a discrete change in the control parameters each hop.

Finally, in Chapter 5 we extend the control method used for the two-mass robot to a three-link robot hopping on an elastic ground. Similar to the two-mass hopping robot the hybrid controller utilizes a continuous control strategy based on backstepping to control the energy of the robot. Then the control parameters are discretely changed at each hop to stabilize the system to the desired apex height.

The results of simulations show that the presented control strategies are capable of achieving a repeated apex height for each hopping robot. Furthermore, the experimental results show the control strategy is capable of achieving the desired apex height even in the prescience of uncertainty. In Chapter 6 we present the conclusions.

Chapter 2

Two-Mass Hopping Robot on a Rigid Foundation

During normal walking and running, a humanoid robot must interact with the ground. The most common ground is considered to be rigid, i.e. it does not deform when the robot makes contact with it. The rigid ground assumption also implies that the robot makes inelastic contact with the ground, i.e. the velocity of the point of contact of the robot immediately matches that of the ground and goes to zero upon contact

We begin with a simplified model of a hopping legged robot, a two-link prismatic joint robot. The two-link robot effectively acts as two masses connected through an applied for. The addition of the lower mass allows you to account for the loss of energy due to impact. The control objective is to achieve a motion which produces a desired value of the center of mass at the highest point of the hop, or apex height. A hybrid control strategy consisting of a continuous and discrete controller is implemented in order to achieve the the objective of a desired apex height. Experiments are presented to validate the control strategy. The control method for the two-mass robot is then extended for use with a four link robot.

The two mass hopping robot utilizes two masses with an actuated force between them. This is slightly more complicated than the inverted pendulum models which instead allow for application of the force directly at the point of contact at the base rather than the base

mass. The control method presented follows the results of Mathis and Mukherjee [21] and [22].

2.1 Dynamics

2.1.1 Coordinate System Description

Consider the hopping robot shown in Fig. 2.1. It is comprised of two masses, m_1 and m_2 (first and second mass, respectively), which are connected by a linkage. The force applied by the linkage on the two masses, denoted by F, can be actively controlled. The height of second mass with respect to the ground is denoted by x, and the height of the first mass with respect to the second mass is denoted by y. Both x and y are assumed positive in the vertically upward direction. The force applied by the ground on the mass is denoted by F_{ext};

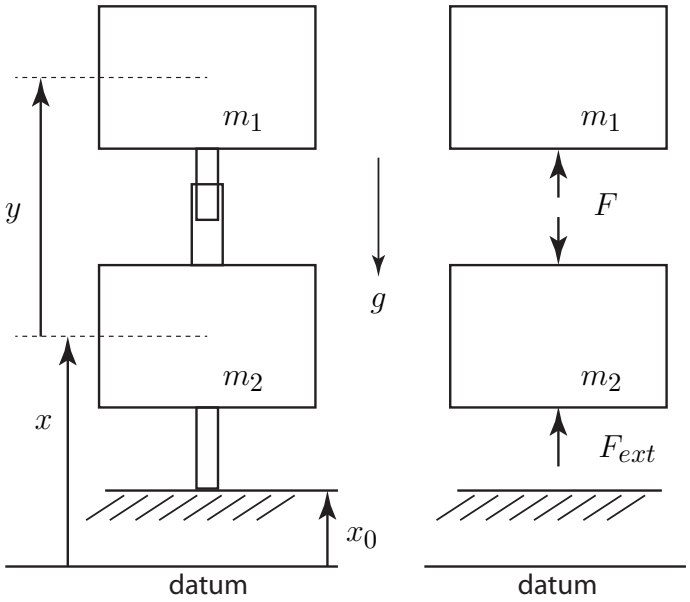

Figure 2.1: Two-mass hopping robot

in the flight phase $F_{ext} = 0$. The equations of motion of the hopping robot are

$$\begin{aligned} \ddot{x} &= -\frac{1}{m_2}F - g + \frac{1}{m_2}F_{ext} \\ \ddot{y} &= \frac{m_1 + m_2}{m_1 m_2}F - \frac{F_{ext}}{m_2} \end{aligned} \tag{2.1}$$

The values x and $\dot{x}$ are measured with respect to the ground making it impractical for measurement during flight. Thus, It is assumed that only the variables y, $\dot{y}$, and F_{ext} can be measured, and our objective is to control the height of the center of mass to a desired value. The hybrid dynamics of the hopping robot is comprised of three distinct phases: the flight phase, the inelastic impact, and the contact phase.

2.1.2 Flight Phase

During the flight phase, the system is not in contact with the ground and therefore

$$x > x_0, \qquad F_{ext} = 0 \tag{2.2}$$

2.1.3 Inelastic Impact

At the instant when the second mass comes in contact with the ground the system moves from $x > 0$ to $x = 0$. At this instant we assume the following to hold true:

Assumption 1. The impact between the second mass with the ground results in an instantaneous change in the velocities of the system, $\dot{x}$ and $\dot{y}$. The impulsive force applied by the ground on the second mass is denoted by

$$F_{ext} = F_{imp} \tag{2.3}$$

Assumption 2. The control force F is not impulsive in nature.

Assumption 3. The collision of the second mass with the ground is inelastic.

If t_c denotes the time in which the second mass comes in contact with the ground, assumption 3 implies

$$\lim_{t \to t_c^+} \dot{x}(t) = 0 \tag{2.4}$$

Using the dynamics given in Eq.(2.1) and assumptions 1 and 2, we get

$$F_{imp} = \lim_{t \to t_c^-} m_2 \dot{x}(t) \tag{2.5}$$

and

$$\lim_{t \to t_c^+} \dot{y} = \lim_{t \to t_c^-} [\dot{y} + \dot{x}] \tag{2.6}$$

from Eq.(2.4) and (2.6) The impulsive dynamics can be described by the mapping

$$\lim_{t \to t_c^+} \begin{bmatrix} y \\ \dot{y} \\ x \\ \dot{x} \end{bmatrix} = S \lim_{t \to t_c^-} \begin{bmatrix} y \\ \dot{y} \\ x \\ \dot{x} \end{bmatrix}, \; S \triangleq \begin{bmatrix} 1 & 0 & 0 & 0 \\ 0 & 1 & 0 & 1 \\ 0 & 0 & 1 & 0 \\ 0 & 0 & 0 & 0 \end{bmatrix} \tag{2.7}$$

2.1.4 Contact Phase

The contact phase defines the period of time during which the second mass remains in contact with the ground. For the contact phase we make the following assumptions

Assumption 4. The external force exerted on the system acts in the positive direction only

(the ground is not sticky), and therefore

$$F_{ext} \geq 0 \tag{2.8}$$

Assumption 5. The environment is rigid and therefore,

$$x \equiv x_0 \tag{2.9}$$

Using assumptions 4 and 5, F_{ext} can be computed as

$$F_{ext} = m_2 g + F \geq 0 \tag{2.10}$$

Substituting Eq.(2.10) into (2.1) we obtain the dynamics of contact phase:

$$\begin{aligned} \ddot{y} &= -g + \frac{1}{m_1} F \\ \ddot{x} &= 0 \end{aligned} \tag{2.11}$$

At the instant when the system switches from the contact phase to the flight phase, F_{ext} crosses zero and therefore

$$F_{ext} = F + m_2 g = 0 \tag{2.12}$$

2.2 Continuous Control of the Height of the Center-of-Mass

2.2.1 Feedback Linearization

If z denotes the height of the center of mass of the hopping robot, we can write

$$z = x + x_0 + m_f y, \qquad m_f \triangleq \frac{m_1}{m_1 + m_2} \tag{2.13}$$

Since the measurement of x is not available, we define the height of the center of mass relative to the second mass by r which can be written as

$$r = (z - x - x_0) = m_f y \tag{2.14}$$

Differentiating Eq.(2.14) twice, we get

$$\ddot{r} = \frac{1}{m_2}[F - m_f F_{ext}] \tag{2.15}$$

To control the value of r we choose the control input F as follows

$$F = m_f F_{ext} + m_2 v \tag{2.16}$$

where v will be chosen later. Substitution of Eq.(2.16) into Eq.(2.15) results in

$$\ddot{r} = v \tag{2.17}$$

The choice of v for the flight phase and the contact phase is discussed next.

2.2.2 Flight Phase

The dynamics of the hopping robot during flight phase is given by the relations

$$\begin{aligned} \ddot{z} &= -g \\ \ddot{r} &= v \end{aligned} \tag{2.18}$$

We seen from Eq.(2.18) that the dynamics of z is independent of the control force and is therefore uncontrollable. To control the position of the relative center of mass, we choose v as follows

$$v = -K(r - r_d) - D\dot{r} \tag{2.19}$$

where $r_d > 0$ is some constant, and K and D are constant proportional and derivative gains. The choice of v in (2.19) results in the dynamics

$$\ddot{r} + D\dot{r} + K(r - r_d) = 0 \tag{2.20}$$

which implies that the equilibrium $(r, \dot{r}) = (r_d, 0)$ is asymptotically stable.

2.2.3 Contact Phase

During the contact phase, $x \equiv x_0$ and therefore

$$\begin{aligned} z &= r \\ \ddot{r} &= v \end{aligned} \tag{2.21}$$

Since $x \equiv 0$, the dynamics of the system is reduced from order 4 to order 2. To emulate a natural hopping motion we design v as follows

$$v = \begin{cases} -K(r - r_d) - D\dot{r} & \dot{r} \leq 0 \\ -K(r - r_d) - \nu D\dot{r} & \dot{r} > 0 \end{cases} \tag{2.22}$$

where D chosen as follows

$$0 < D < 2\sqrt{K} \tag{2.23}$$

Such a choice of D allows the first mass to behave as an under-damped oscillator during its downward motion. By choosing $\nu < 0$ we ensure that the first mass behaves like a negatively damped oscillator and energy can be added to the system during its upward motion. The amount of energy added will depend on the choice of ν and this will be determined based on the desired maximum height of z and its current value. This will be discussed in the section on discrete control.

2.2.4 Hybrid Dynamics of Closed-Loop System

The hybrid dynamics of the closed-loop system can be summarized as follows:

Flight Phase: Substituting Eqs.(2.16), (2.18), and (2.19) into (2.1) and setting $F_{ext} = 0$, we have

$$\begin{aligned} \ddot{x} &= K\left[m_f y - r_d\right] + Dm_f\dot{y} - g \\ \ddot{y} &= -K\left[y - \frac{1}{m_f}r_d\right] - D\dot{y} \end{aligned} \tag{2.24}$$

Impact: The impulsive dynamics is described by the mapping in Eq.(2.7)

Contact phase: Substituting Eqs.(2.10), (2.16), (2.21), and (2.22) into (2.1), we have

$$\begin{aligned} x &\equiv x_0 \\ \ddot{y} &= -K(y - \frac{1}{m_f} r_d) - \mu D \dot{y} \end{aligned} \tag{2.25}$$

where

$$\mu = \begin{cases} 1 & \dot{r} \leq 0 \\ \nu & \dot{r} > 0 \end{cases} \tag{2.26}$$

2.3 Poincaré Map

2.3.1 Construction of First Return Map

We define the first return as the mapping over a single hop starting from liftoff and ending at the next liftoff. Without loss of generality, we consider the time of first liftoff to be $t = 0$, and Δt_1, Δt_2, and Δt_3 to be the durations of the flight phase, contact phase with downward velocity of the first mass, and contact phase upward velocity of the first mass respectively. For convenience, we define

$$\begin{aligned} T_1 &= \Delta t_1 \\ T_2 &= \Delta t_1 + \Delta t_2 \\ T_3 &= \Delta t_1 + \Delta t_2 + \Delta t_3 \end{aligned} \tag{2.27}$$

and the state vector as follows

$$X(t) = [y(t), \quad \dot{y}(t), \quad x(t), \quad \dot{x}(t)]^T \tag{2.28}$$

Using Eq.(2.24), the states of the system at the end of the flight phase can be obtained as follows

$$X(T_1) = \begin{bmatrix} e^{A_f \Delta t_1} & 0 \\ -m_f e^{A_f \Delta t_1} & 0 \end{bmatrix} X(0) + B_f \tag{2.29}$$

where A_f and B_f are given by the relations

$$A_f = \begin{bmatrix} 0 & 1 \\ -K & -D \end{bmatrix} \qquad B_f = \begin{bmatrix} B_{f1} \\ -B_{f1} + B_{f2} \end{bmatrix} \tag{2.30}$$

and B_{f1} and B_{f2} are given by

$$\begin{aligned} B_{f1} &= \int_0^{\Delta t_1} e^{A_f(\Delta t_1 - \tau)} K \frac{1}{m_f} R \, d\tau \\ B_{f2} &= \begin{bmatrix} m_f[y(0) + \dot{y}(0)\Delta t_1] - \frac{1}{2} g (\Delta t_1)^2 \\ m_f \dot{y}(0) \Delta t_1 - g \Delta t_1 \end{bmatrix} \end{aligned} \tag{2.31}$$

and R is given by

$$R = [0 \quad r_d \quad 0 \quad 0]^T \tag{2.32}$$

Immediately following the flight phase the system impacts the ground and the states change according to Eq.(2.7). Following the impact the first mass descends downward in the contact phase. The states of the system, when the first mass has reached the lowest vertical position, are obtained from Eqs.(2.25) and (2.26) as follows

$$X(T_2) = e^{A_c \Delta t_2} S X(T_1) + B_c \tag{2.33}$$

where A_c and B_c are given by the relations

$$A_c = \begin{bmatrix} 0 & 1 & 0 & 0 \\ -K & -D & 0 & 0 \\ 0 & 0 & 0 & 1 \\ 0 & 0 & 0 & 0 \end{bmatrix} \tag{2.34}$$

$$B_c = \int_{T_1}^{T_2} e^{A_c(T_2-\tau)} K \frac{1}{m_f} R \; d\tau \tag{2.35}$$

Using Eqs.(2.25) and (2.26) again, the states at liftoff are obtained as

$$X(T_3) = e^{A_p \Delta t_3} X(T_2) + B_p \tag{2.36}$$

where A_p and B_p are given by the relations

$$A_p = \begin{bmatrix} 0 & 1 & 0 & 0 \\ -K & -\nu D & 0 & 0 \\ 0 & 0 & 0 & 1 \\ 0 & 0 & 0 & 0 \end{bmatrix} \tag{2.37}$$

$$B_p = \int_{T_2}^{T_3} e^{A_p(T_3-\tau)} K \frac{1}{m_f} R \; d\tau \tag{2.38}$$

Substituting Eqs.(2.29) and (2.33) into Eq.(2.36) gives the mapping for the configuration of the first mass over one hop. This mapping is given bellow

$$\begin{bmatrix} y(T_3) \\ \\ \dot{y}(T_3) \end{bmatrix} = P\left[X(0), \Delta t_1, \Delta t_2, \Delta t_3\right] \tag{2.39}$$

2.3.2 Period One Orbits

Equation (2.39) gives the first return map for one hop. Indexing each hop by an integer we may write without loss of generality

$$\chi(0) = \begin{bmatrix} y(0) \\ \\ \dot{y}(0) \end{bmatrix} \tag{2.40}$$

and

$$\chi(1) \;\; = \;\; \begin{bmatrix} y(T_3) \\ \\ \dot{y}(T_3) \end{bmatrix} = P\left[X(0), \Delta t_1, \Delta t_2, \Delta t_3\right] \tag{2.41}$$

The discrete dynamics of the hopping motion is therefore

$$\chi(k+1) = P[\chi(k)] \tag{2.42}$$

where the dependence on $(\Delta t_1, \Delta t_2, \Delta t_3)$ has been dropped since they all depend on $\chi(k)$. In particular, for the first hop, Δt_1, Δt_2, and Δt_3 can be solved using the following equations:

$$\begin{aligned} x(T_1) &= x_0 \\ \dot{y}(T_2) &= 0 \\ -K[y(T_3) - \frac{1}{m_f} r_d] - \nu D\dot{y}(T_3) + \frac{g}{m_f} &= 0 \end{aligned} \tag{2.43}$$

The meaning of the first two equations above are clear. The third equation is obtained by setting $F_{ext} = 0$ at the time of liftoff. A period-one hop of the system correspond to equilibrium point of the discrete system in equation (2.42) which are the points χ which satisfy

$$\chi(k+1) = \chi(k) = P[\chi(k)] \tag{2.44}$$

Equation (2.43) and (2.44) may then be solved numerically to find all the period one orbits of the system for a given ν value.

2.3.3 Stability Analysis of First Return Map

Once the periodic point for each ν value are determined, it is necessary to determine the stability of each point. To do so we linearize the discrete system in equation (2.42) about a given periodic point, denoted by χ^*, giving

$$\chi(k+1) \approx P(\chi^*) + \frac{dP(\chi)}{d\chi}|_{\chi=\chi^*}(\chi(k) - \chi^*) \tag{2.45}$$

where the Jacobian matrix $\frac{dP(\chi)}{d\chi}$ is obtained by implicit differentiation of Eq.(2.43). By defining the error between the current point of liftoff with the periodic point as

$$E(k) = \chi(k) - \chi^* \tag{2.46}$$

we have the linearized equation of the discrete dynamics:

$$E(k+1) \approx \frac{dP(\chi)}{d\chi} E(k) \tag{2.47}$$

The periodic point is asymptotically stable if and only if

$$\rho\left[\frac{dP(\chi)}{d\chi}\right] < 1 \tag{2.48}$$

where $\rho[\bullet]$ is the spectral radius.

2.4 Discrete Control

2.4.1 Mapping Between Apex Height and Liftoff Configuration

The height to which the hopper will jump (the maximum value of z denoted here by h) depends on the value of y and $\dot{y}$, or alternatively r and $\dot{r}$, at the time of lift off, *i.e.*, $h = h(\chi)$. To find this functional representation we realize that the total energy (kinetic plus potential) of the center of mass remains constant during the flight phase, *i.e.*

$$E(\chi) = \frac{1}{2}(m_1 + m_2)\dot{z}^2 + (m_1 + m_2)g\ z = \text{const.} \tag{2.49}$$

Note that z and $\dot{z}$ are identical to r and $\dot{r}$ at the time of lift-off. The second equation needed to determine the value value of h is $F_{ext} = 0$ at lift-off. Defining the map $T(\chi^*, \nu^*)$ as

$$T(\chi^*, \nu) = \begin{bmatrix} \frac{1}{(m_1+m_2)g} E(\chi^*) \\ F_{ext}(\chi^*, \nu^*) \end{bmatrix} = \begin{bmatrix} h \\ 0 \end{bmatrix} \tag{2.50}$$

we can solve for χ^* for a given value of h as follows

$$\chi^* = T^{-1}(h, \nu^*) \tag{2.51}$$

Note that ν is the only variable over which we have control. Therefore, our objective is to determine the right value of $\nu = \nu^*$ that will make the hopper jump to the desired height.

2.4.2 Stabilizing the Liftoff Configuration

Equations (2.44) and (2.51) produce a set of points (χ^*, ν^*) which are periodic and have a hopping height h. To ensure asymptotic convergence of the hopper to the desired periodic point, or equivalently to the desired hopping height, we change ν to a different constant value for each hop. Linearizing the discrete dynamics in Eq.(2.44) about the periodic point (χ^*, ν^*) gives

$$\begin{aligned} \chi(k+1) = P(\chi^*, \nu^*) &+ \frac{dP(\chi, \nu)}{d\chi}|_{\chi=\chi^*, \nu=\nu^*}(\chi(k) - \chi^*) \\ &+ \frac{dP(\chi, \nu)}{d\nu}|_{\chi=\chi^*, \nu=\nu^*}(\nu(k) - \nu^*) \end{aligned} \tag{2.52}$$

where the Jacobian matrices $\frac{dP(\chi,\nu)}{d\chi}$ and $\frac{dP(\chi,\nu)}{d\nu}$ are determined by implicit differentiation of Eq.(2.43). Defining the error and control input states $E(k)$ and $U(k)$ as

$$\begin{aligned} E(k) &= \chi(k) - \chi^* \\ U(k) &= \nu(k) - \nu^* \end{aligned} \tag{2.53}$$

and using equation (2.44) we may write the linearized dynamics as

$$\begin{aligned} E(k+1) &= \frac{dP(\chi,\nu)}{d\chi}|_{\chi=\chi^*,\nu=\nu^*} E(k) \\ &\quad + \frac{dP(\chi,\nu)}{d\nu}|_{\chi=\chi^*,\nu=\nu^*} U(k) \end{aligned} \tag{2.54}$$

Choosing the control action to be

$$U(k) = CE(k) \quad \Rightarrow \quad \nu(k) = \nu^* + CE(k) \tag{2.55}$$

where C is a constant matrix. We find the choice of the matrix C such that

$$\rho\left[\frac{dP}{d\chi}|_{\chi=\chi^*,\nu=\nu^*} + \frac{dP}{d\nu}|_{\chi=\chi^*,\nu=\nu^*} C\right] < 1 \tag{2.56}$$

asymptotically stabilizes the system to the desired periodic point.

2.5 Simulations

The two masses of the hopper are assumed to be

$$m_1 = 50 \text{ kg} \quad m_2 = 20 \text{ kg} \tag{2.57}$$

The desired height h and r_d are chosen as

$$h = 2 \text{ m} \quad r_d = 1.071 \text{ m} \tag{2.58}$$

Note that the value of $r = 1.071$ corresponds to a value of $y = 1.5$. We assume the ground height to be

$$x_0 = 0.2 \text{ m} \tag{2.59}$$

This results in resting height of the center-of-mass of the hopper to be 1.271 meters above the datum. The continuous control gains K and D are chosen to be

$$K = 1500 \text{ N/(kg m)} \quad D = 10 \text{ Ns/(kg m)} \tag{2.60}$$

The values of K and D satisfy $D < 2\sqrt{K}$ discussed earlier. For the parameters presented, Fig.2.2 provides numerical solutions for the hopping height associated with period one orbits, *i.e.*, solutions to Eqs.(2.44) in terms ν. Note that there are multiple heights associated with a given value of ν, and this makes the choice of a ν associated with the desired height difficult. We see that there appears to be a minimum value of h for a given ν. This is understood as there is a minimum height that the center of mass must reach in order for the system to hop and thus produce a return map.

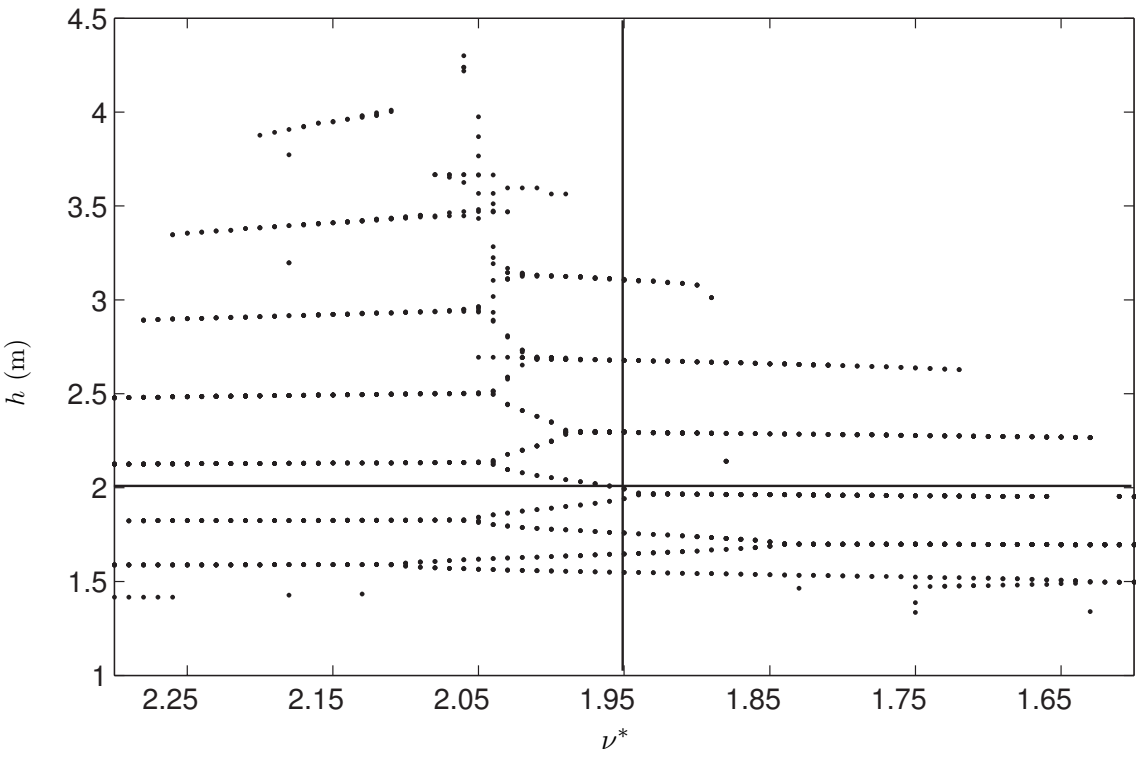

Figure 2.2: Apex height h corresponding to periodic orbits of the system for a given ν^* value

For the desired height of $h = 2$ we used Fig.(2.3) to determine

$$\nu^* = -1.95 \tag{2.61}$$

A discrete LQR problem was solved to determine the control gains in Eq.(2.55). These gains are given below

$$C = [-0.0780 \quad -0.1618] \tag{2.62}$$

The given ν^* and desired height h determine the lift off values x^*, and the gains C asymptotically stabilize the system to the given x^* and thus the desired height. The initial conditions,

without loss of generality, were assumed to be

$$x(0) = 0.2 \text{ m} \quad \dot{x}(0) = 0 \text{ m/s}$$
$$y(0) = 1.5835 \text{ m} \quad \dot{y}(0) = 6 \text{ m/s} \tag{2.63}$$

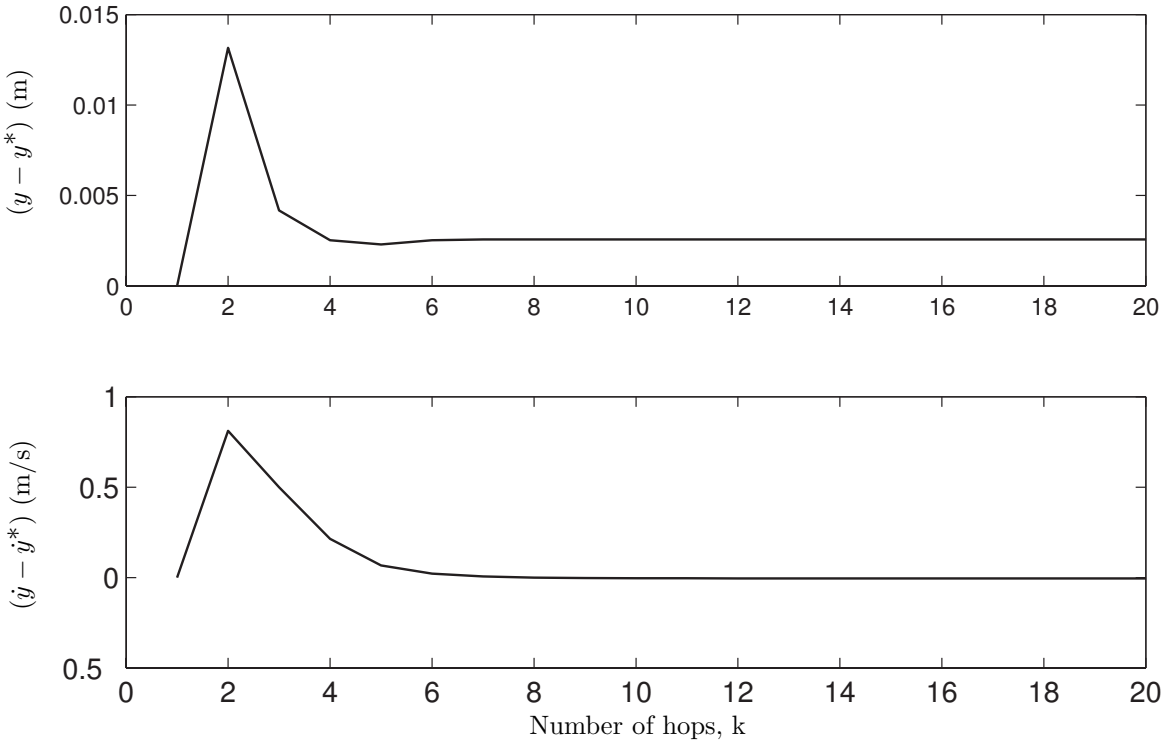

Figure 2.3: Error between desired lift-off states χ^* and actual lift-off states at the kth-hop $\chi(k)$

Figure 2.3 plots the error between the desired periodic point χ^*, and the actual lift-off point $\chi(k)$ for each hop. The system converges in approximately 8 hops. However, we note that the control results in steady state error. This is due to inexact estimation of ν^* from Fig.2.2. Figure 2.4 shows the height of the first mass, second mass, and center of mass above the ground. We see that the peak height of the center of mass converges to approx. 2 meters as prescribed by the control objective.

From the simulations we see that efficacy of the control algorithm. However, to further

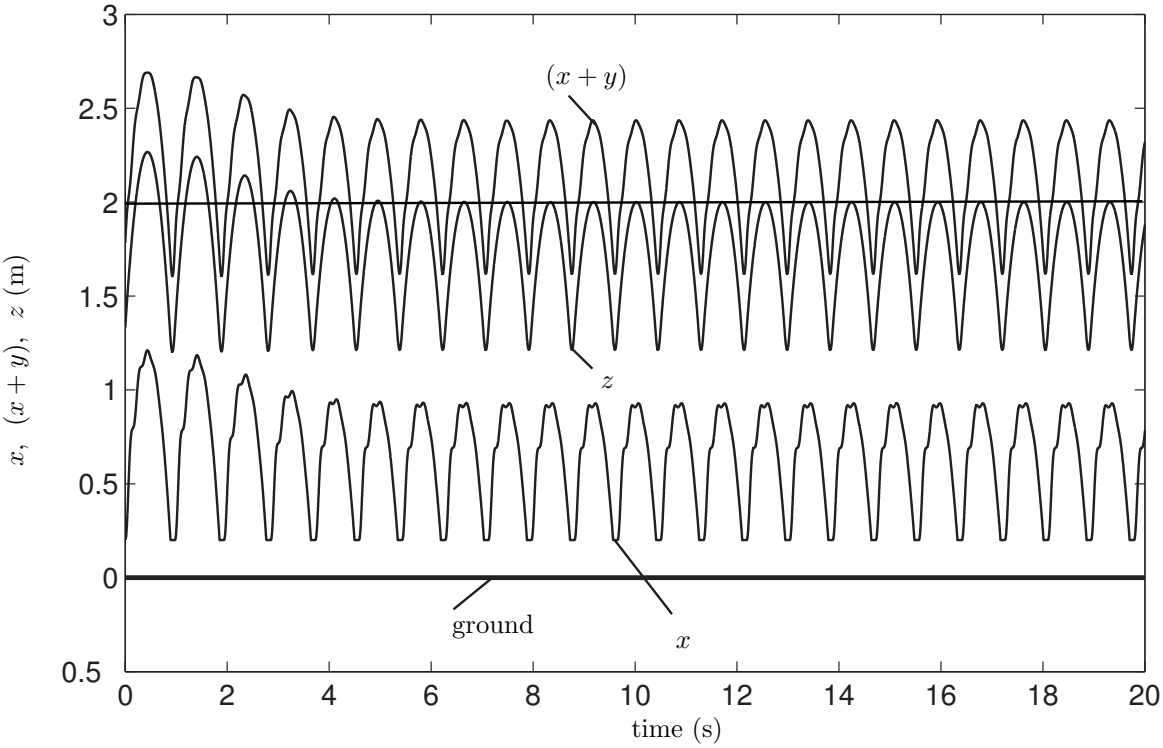

Figure 2.4: Absolute height of the two masses m_1 and m_2, and center-of-mass height are plotted as a function of time

investigate the robustness and applicability of the control algorithm, it behooves us to experimentally test the control method. Therefore, in the next section we will discuss the design, application, and results of a two mass hopping robot experiment.

2.6 Two-Mass Hopper Experiments

In Chapter 2, section 2 we presented a method of controlling the apex height of a two mass hopping robot. To expand of the efficacy of the presented algorithm, we will now investigate an experimental robot that is controlled via the presented algorithm.

2.6.1 Description of Experimental Hardware

In the experimental setup, the two-mass hopper is comprised of a voice-coil actuator and two linear guides - see Fig.2.5. One linear guide is connected to the coil housing of the voice-coil actuator and together they make up the lower mass of the hopper. The other linear guide is connected to the cylindrical permanent magnet of the voice-coil actuator and together they make up the upper mass of the hopper. Both linear guides are mounted to the vertical rail; this constrains the upper and lower masses to move in the vertical direction and prevents collision between them. The voice-coil actuator is a product of Moticont [1]; it serves as a linear motor, and for a commanded input current it outputs a force between the upper and lower masses with a gain of 10.6 N/A. It has a stroke length of 0.1334 m and has the capability to apply a continuous force of 21.5 N and an intermittent force of 68.1 N (10% duty cycle). The position of the two masses are measured by two linear encoders whose scale is mounted on the other vertical member; the encoders are a product of US Digital [4] and they have a resolution of 120 lines/inch. The current in the voice-coil is provided by a motor controller [2] powered by a 80 volt power supply. A DS1104 dSpace board [3], residing in a host personal computer, is used for data acquisition and real-time control. The mass and length parameters of the hopper are given by.

$$m_1 = 2.668 \text{ kg}, \quad m_2 = 0.808 \text{ kg}, \quad \ell = 0.059 \text{ m} \tag{2.64}$$

2.6.2 Control Implementation in Experiments

The continuous controller defined by (2.16), (2.24), (2.25) and (2.26) requires the knowledge of the external force F_{ext} during the contact phase. The external force can be measured

directly using a force sensor but such a sensor is not present in our experimental hardware. To overcome this problem, we substitute (2.9) and (2.1) into (2.16) to rewrite the control force in the contact phase as follows

$$\begin{aligned} & F = m_{\mathrm{f}}(F + m_2 g) + m_2 v \\ \Rightarrow \quad & F = \frac{m_2(m_{\mathrm{f}} g + v)}{1 - m_{\mathrm{f}}} \end{aligned} \tag{2.65}$$

It can be verified from (2.13) that $m_{\mathrm{f}} < 1$; the force in (2.65) is therefore non-singular. The parameters of the continuous controller were chosen to be the same as those in simulation which are given in (2.71). The choice of the value of $r_{\mathrm{d}} = 0.0979$ m can be explained as

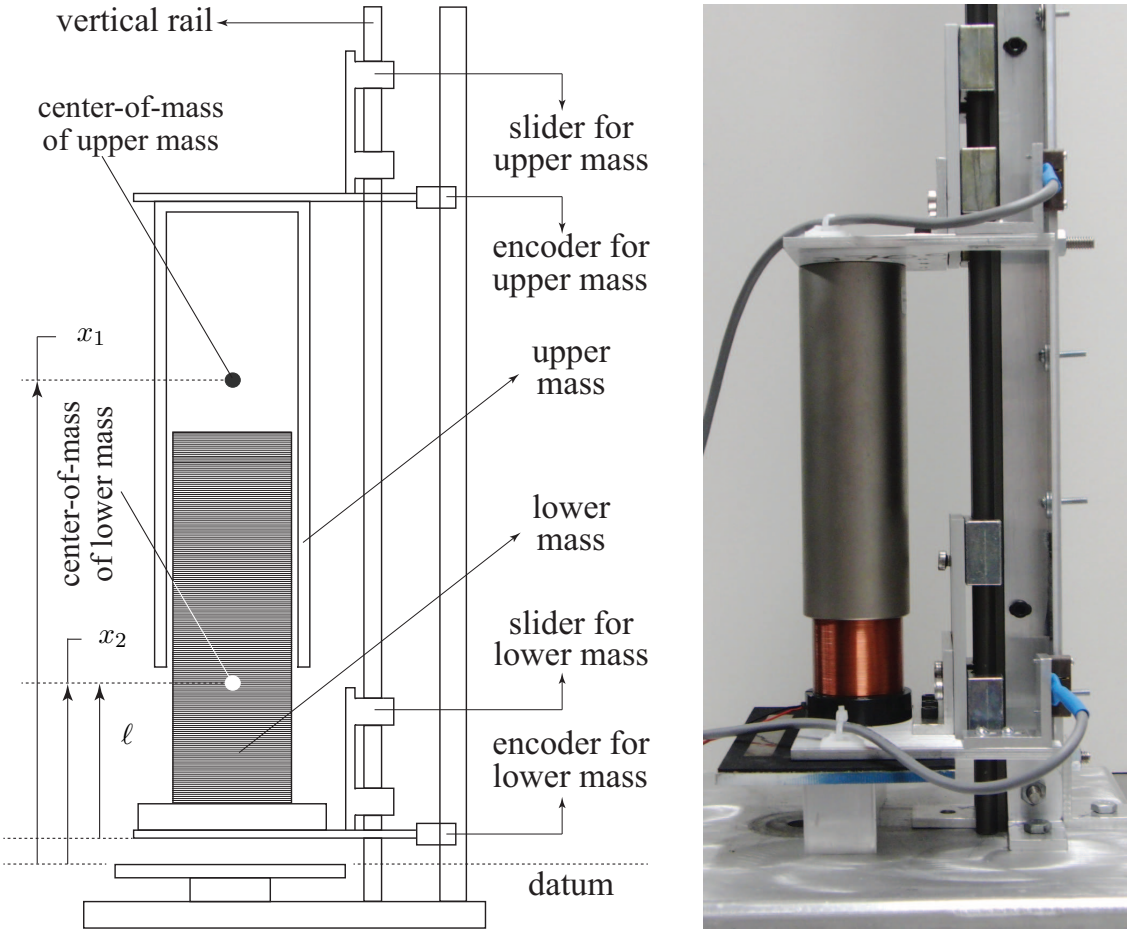

Figure 2.5: Schematic (left) and photograph (right) of the experimental hardware.

follows: In the shortest length configuration, the upper and lower masses of the voice-coil are separated by a distance of $y_{\min} = 0.064$ m. The maximum stroke length of the voice-coil is 0.1334 m but the force decays rapidly at the end of its stroke. The active stroke length of the voice-coil is the length over which the force can be accurately controlled; this is equal to $s_{\max} = 0.127$ m as per the specifications of the manufacturer [1]. By choosing half the stroke length as the desired neutral position of the hopper, the value of r_{d} is determined as

$$r_{\mathrm{d}} \triangleq m_{\mathrm{f}}\, y_{\mathrm{d}} = \frac{m_1}{(m_1 + m_2)}\,(y_{\min} + \frac{1}{2} s_{\max}) = 0.0979$$

The desired apex height was chosen to be

$$h_{\mathrm{des}} = 0.213 \text{ m} \tag{2.66}$$

The fixed point (ξ^*, ν^*) and gain C for the discrete controller were chosen from the simulation.

2.6.3 Poincaré Map Reduction

The Poincare map, $P(\chi, \nu)$ depends on the states (χ, ν) where the states χ are given by

$$\chi \in \Omega, \qquad \Omega = \{(y,\ \dot{y}) \in \mathbb{R}^2 \ \mid x = 0,\ \dot{x} = 0,\ F_{ext} = 0\} \tag{2.67}$$

Which implies that the Poincare map is a homeomorphism on R^3. However, We note that at the instant of liftoff, the forces F and F_{ext} are given by

$$
\begin{aligned}
F &= m_f F_{ext} + m_2 v \\
v &= -K\left[m_f y - r_d\right] - \nu D m_f \dot{y} \\
F_{ext} &= F + m_2 g = 0
\end{aligned} \tag{2.68}
$$

Combining Eqns.(2.68) and solving for y gives

$$
y = \frac{g - \nu D m_f \dot{y}}{K m_f} + \frac{r_d}{m_f} \tag{2.69}
$$

Equation (2.69) means that the dimensionality of the return map may be reduced. Namely that we may write $P(\xi, \nu)$ where

$$
\xi \in \Lambda, \quad \Lambda = \{\dot{y} \in \mathbb{R} \mid x = 0,\ \dot{x} = 0,\ F_{ext} = 0,\ y = \frac{g - \nu D m_f \dot{y}}{K m_f} + \frac{r_d}{m_f}\} \tag{2.70}
$$

From Eqn.(2.70) we see that the Poincare map, $P(\xi, \nu)$ is actually a homeomorphism on $\mathbb{R}^2$. The the experimental application we will use the the map on (ξ, ν) rather than the map on (χ, ν).

2.6.4 Simulation Results with Hardware Parameters

The mass and length parameters of the hopper were assumed to be the same as those in our experimental setup - see (2.64).

The parameters of the continuous controller were chosen as

$$K = 600 \text{ s}^{-2}, \quad D = 5 \text{ s}^{-1}, \quad r_{\text{d}} = 0.0979 \text{ m} \tag{2.71}$$

The choice of r_{d} is the same as that used in experiments and will be explained later in section 2.6.2.

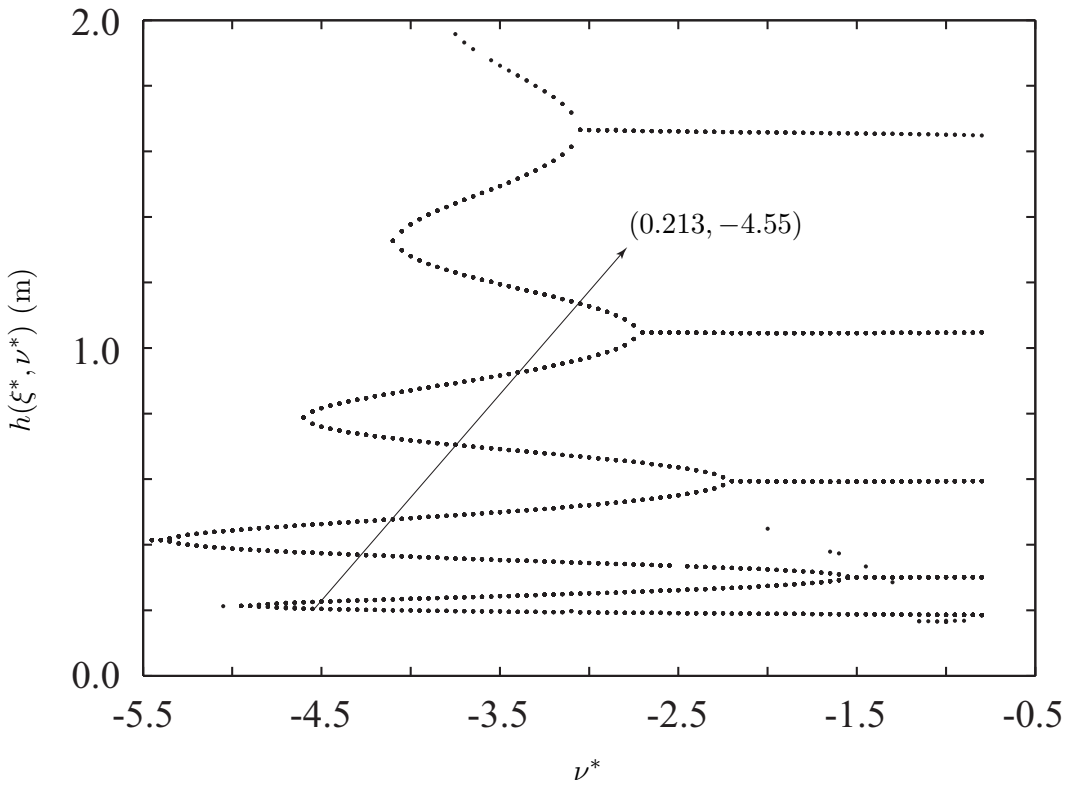

Figure 2.6: Apex height h corresponding to periodic orbits of the system obtained with different values of ν.

The discrete controller parameter ν requires us to choose a nominal value ν^*, where ν^* corresponds to the fixed point (ξ^*, ν^*). A numerical search was used to find as many fixed points (ξ^*, ν^*) as possible. Each fixed point corresponds to a unique value of $h = h(\xi^*, \nu^*)$ and Fig.2.6 plots these fixed points in the h-ν plane. This plot is useful for choosing ν^* for a desired value of $h = h_{\text{des}}$. Our desired apex height is given in (2.66)

From Fig.2.6, this corresponds to

$$\nu^* = -4.55 \tag{2.72}$$

For these values of h_{des} and ν^*, the value of ξ^* was

$$\xi^* = \dot{y} = 0.76 \text{ m/s} \tag{2.73}$$

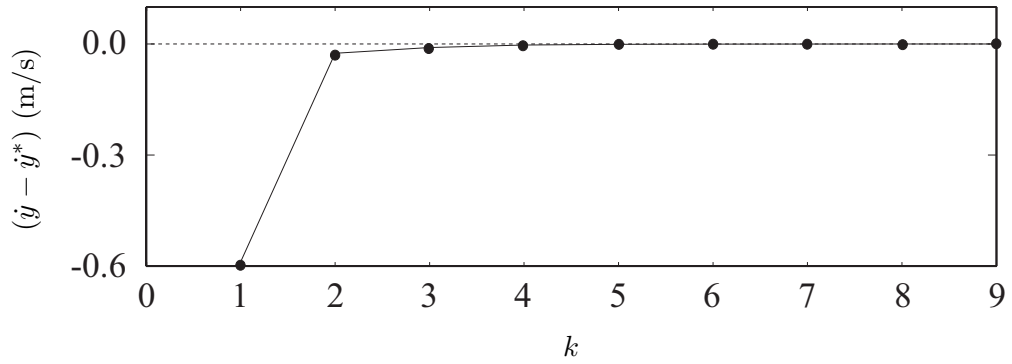

Figure 2.7: Simulation results: Error between the actual lift-off state $\xi = \dot{y}$ and the desired lift-off state $\xi^* = \dot{y}^*$ at the beginning of the k-th hop, $k = 1, 2, \cdots, 9$.

The gain of the discrete controller was chosen to place the pole at 0.1; the gain was found to be

$$C = -1.08 \tag{2.74}$$

The initial conditions[1] were assumed to be

$$\begin{aligned} x_1(0) &= 0.149 \text{ m}, \quad \dot{x}_1(0) = 0.0 \text{ m/s} \\ x_2(0) &= 0.059 \text{ m}, \quad \dot{x}_2(0) = 0.0 \text{ m/s} \end{aligned} \tag{2.75}$$

and the results are shown here in Figs.2.7, 2.8 and 2.9. Figure 2.7 plots the errors between

[1] These initial conditions are the same as those used in experiments. The value of $x_2(0)$ was chosen to be equal to $\ell = 0.059$ m and the value of $x_1(0)$ corresponds to $y(0) = 0.09$ m.

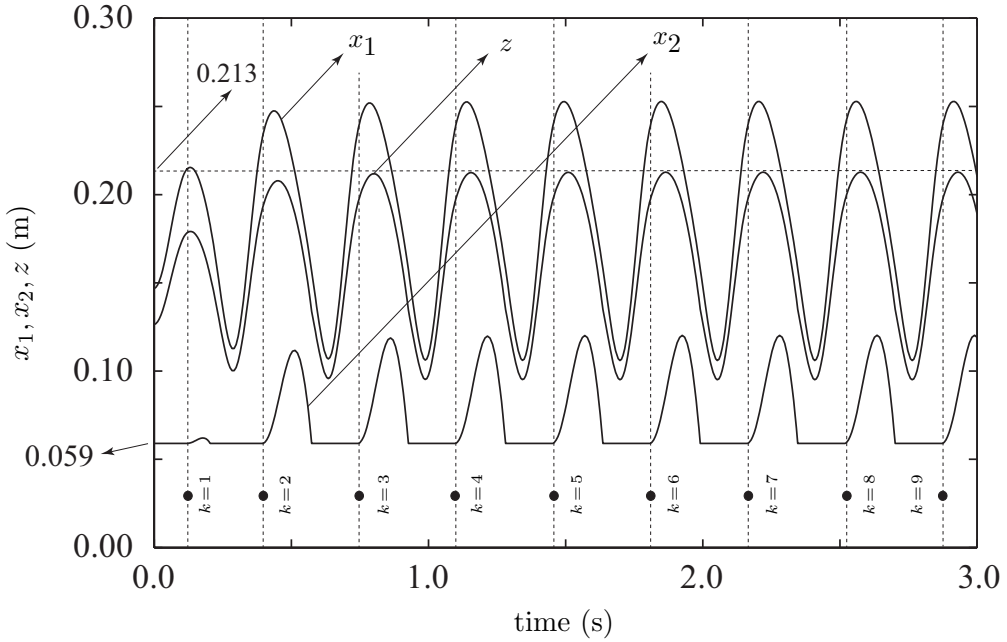

Figure 2.8: Simulation results: Plot of the height of the upper mass x_1, the lower mass x_2, and the center-of-mass z, as a function of time.

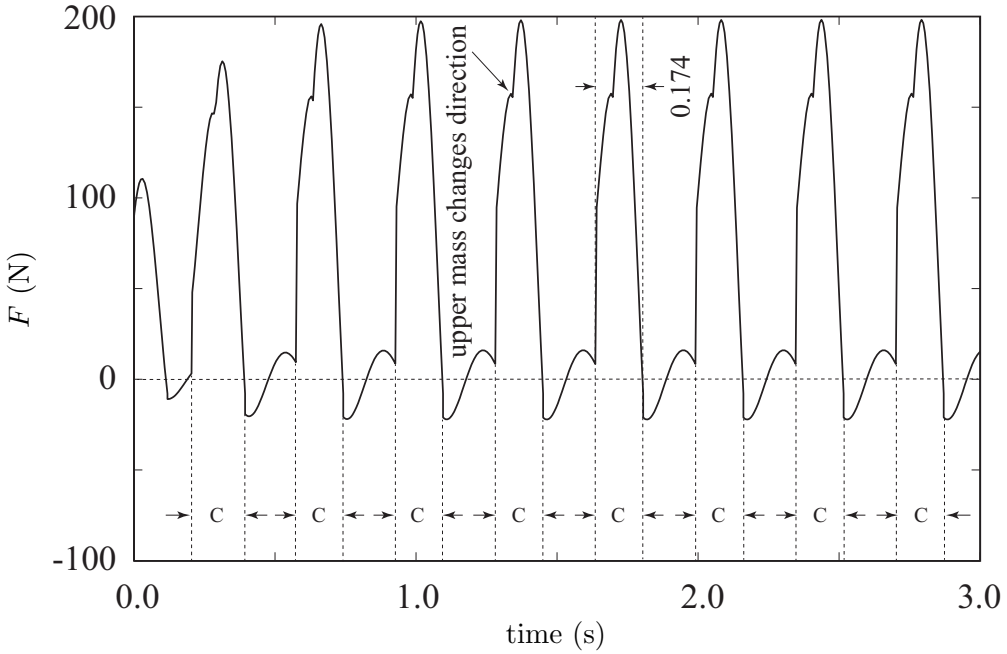

Figure 2.9: Simulation Results: Plot of the force F applied by the actuator.

the actual lift-off state $\xi = \dot{y}$ and desired lift-off state $\xi^* = \dot{y}^*$ as a discrete function of time; the hops are sequentially numbered using the integer variable k and the errors at the

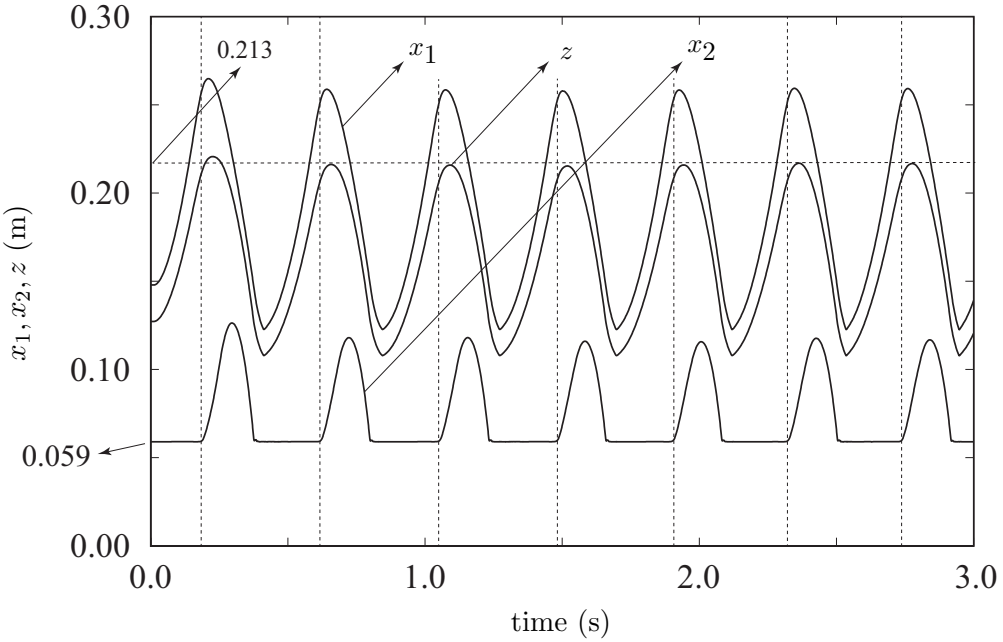

Figure 2.10: Experimental results: Plot of the height of the upper mass x_1, the lower mass x_2, and the center-of-mass z, as a function of time.

beginning of each hop are plotted for $k = 1, 2, \cdots, 9$. It can be seen that the errors become negligible after three hops, *i.e.*, for $k \geq 4$. The positions of the upper mass, lower mass, and center-of-mass of the robot are plotted as a continuous function of time in Fig.2.8. The time intervals during which x_2 remains constant at its lowest value of $\ell = 0.059$ m indicate the contact phases. The robot lift-offs the ground at the end of each contact phase; the discrete instants of time corresponding to $k = 1, 2, \cdots, 9$ in Fig.2.7 are marked by "•" in Fig.2.8. It is clear from Fig.2.8 that the apex height of the robot h (maximum value of z during flight phase) converges to its desired value $h_{\text{des}} = 0.213$ within three hops.

The force applied by the actuator F, defined by (2.16), is shown in Fig.2.9. It can be seen that the actuator force increases significantly during the contact phase. Each contact phase is marked by "c" and the maximum value of the actuator force reaches approximately 200 N, which is slightly larger than 7.5 times the weight of the upper mass m_1. In each contact phase, the upper mass changes direction from downward motion to upward motion.

This change in direction results in the non-smooth control action described by (2.26), which is discernible from Fig.2.9. In the flight phase, the relative motion of the masses is designed to emulate the motion of an under-damped mass-spring damper system; this explains the oscillatory nature of the actuator force. At the beginning of the flight phase, the actuator force is negative since the upper mass lifts the lower mass off the ground.

2.6.5 Comparison of Experimental Results with Simulations

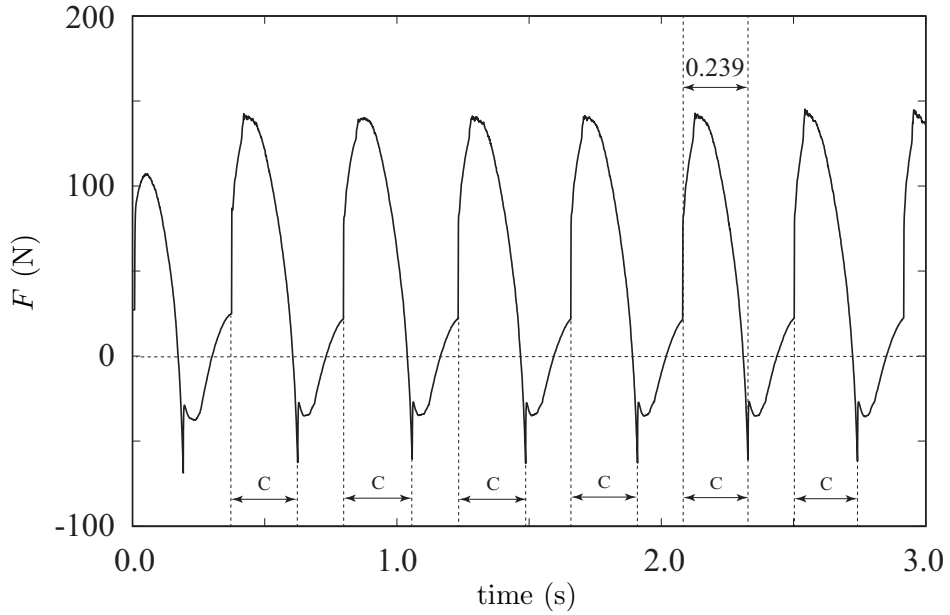

Figure 2.11: Experimental Results: Plot of the force F applied by the actuator.

The experimental results are shown in Figs.2.10 and 2.11 for the same initial conditions as those used in simulations, namely (2.75). Figure 2.10 shows the positions of the upper mass, lower mass, and center-of-mass of the hopper as a continuous function of time; it can be seen that the apex height converges to its desired value in two hops. The control objective is achieved but there are differences between simulation and experimental results. A comparison of Figs.2.8 and 2.10 indicate difference in transient behavior. The apex height gradually increases to its desired value in simulations whereas it overshoots and converges

to its desired value in experiments. The time-period for each hop is also different. In a period of 3 sec, the hopper completes seven hops in experiments but is on its ninth hop in simulations. This is due to the difference in the duration of the contact phases. For example, the contact phase prior to the sixth hop[2] is approx. 0.174 sec in simulation but approx. 0.239 sec in experiment. This is due to the saturation of the actuator force in experiments. A comparison of Figs.2.9 and 2.11 indicate that the peak actuator force is 200 N in simulation but only 150 N in experiments. Since the maximum actuator force is lower in experiments, it is applied for a longer duration in the contact phase such that the hopper can reach the same apex height.

From the experiment we see the validity of the control algorithm presented in Chapter 2.2. Utilizing these results we will next extend the control algorithm from the simplified two mass model to a 4 linked model hopping in a plane.

[2]At the time of the sixth hop, the transient phase is over and the hopper exhibits steady-state hopping behavior in both simulations and experiments.

Chapter 3

Four-Link Hopping Robot on a Rigid Foundation

From the simulation and experimental results of the two-mass hopper in Chapter 2 we see that the control method on rigid ground is capable of achieving a desired apex height for the simplified two-mass system. We now generalize the control methodology to a multi-dof linked robot system. To this end we consider the apex height control of a four-link hopping robot. The choice of a four-link hopping robot is to more closely resemble a humanoid robot.

The control is designed following a similar structure in Chapter 2. Additional consideration is given during both the continuous and discrete phases to account for the additional degrees-of-freedom in the system. The results presented in the chater follow the work of Mathis and Mukherjee [21].

3.1 Dynamics

Consider the four-link, monoped, hopping robot shown in Fig.3.1. Let x and y be the Cartesian coordinates of the base of the foot of the robot (point O) relative to the fixed ground reference. For $i = 1, 2, 3, 4$, the mass, moment of inertia, and length of each link are denoted by m_i, I_i, and l_i respectively. The angular displacement of the ith link is denoted by θ_i and the distance to its center of mass is denoted by d_i - see Fig.3.1. The states are

defined as

$$q = \begin{bmatrix} x & y & \theta_1 & \theta_2 & \theta_3 & \theta_4 \end{bmatrix}^T \tag{3.1}$$

The equations of motion of the hopper are given by

$$M(q)\ddot{q} + N(q, \dot{q}) = AT + F_{ext} \tag{3.2}$$

where $M(q)$ is the mass matrix, $N(q, \dot{q})$ is the vector of Coriolis, centrifugal, and gravitational forces, $A \in \mathbb{R}^{6\times 3}$ is the matrix given below

$$A = \begin{bmatrix} 0 & 0 & 0 & 1 & 0 & 0 \\ 0 & 0 & 0 & 0 & 1 & 0 \\ 0 & 0 & 0 & 0 & 0 & 1 \end{bmatrix}^T, \tag{3.3}$$

T is the vector of input torques

$$T = \begin{bmatrix} \tau_1 & \tau_2 & \tau_3 \end{bmatrix}^T, \tag{3.4}$$

and F_{ext} it the force applied by the ground on the robot given by

$$F_{ext} = \begin{bmatrix} F_x & F_y & 0 & 0 & 0 & 0 \end{bmatrix}^T \tag{3.5}$$

In Eq.(3.5), F_x and F_y denote the x and y components of the force applied to the robot by the ground at point O. The dynamics of the hopper may be separated into three phases: the flight phase for which $y > 0$; the impact phase, which occurs at the first instant when $y = 0$; and the contact phase, which occurs for the duration in which the foot remains in

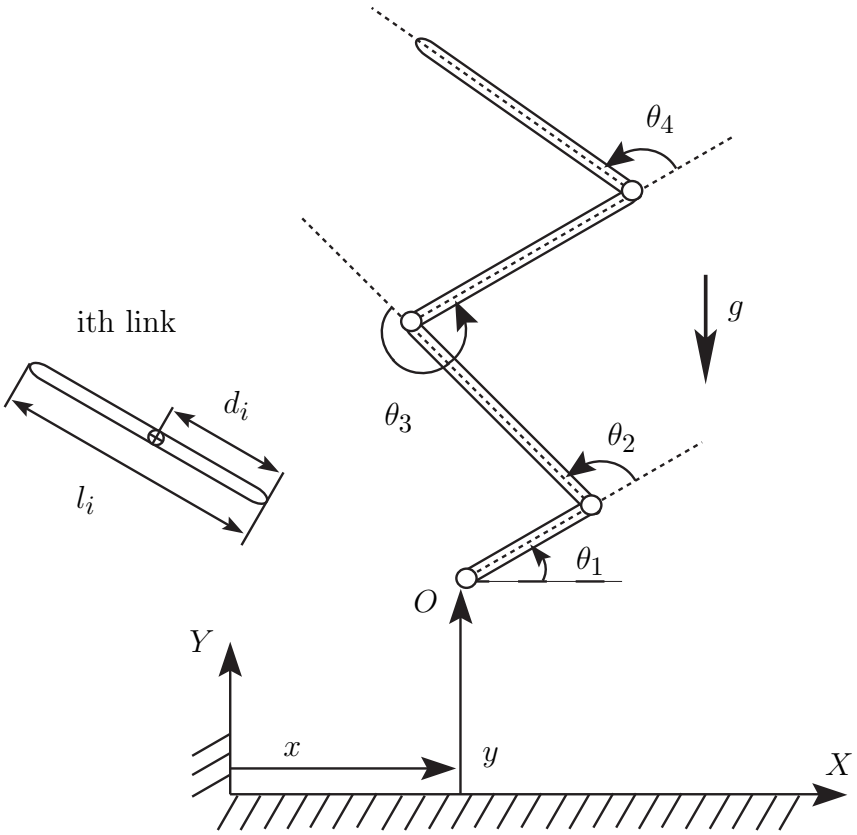

Figure 3.1: Four-link hopping robot

contact with the ground, $y \equiv 0$. The phases mirror those of the two-mass hopper.

3.1.1 Flight Phase

During the flight phase $F_{ext} = 0$. Furthermore, the dynamics in Eq.(3.2) result in the non-holonomic constraint due to conservation of angular momentum about the center of mass of the hopper.

3.1.2 Impact

At the time of impact we assume:

Assumption 1: The applied torques T are not impulsive.

Assumption 1 does not imply that the torques T cannot be discontinuous; it simply

implies that the torques cannot produce discrete jumps in the states.

Assumption 2: The hopper's foot comes in contact with the ground only at point O.

Assumption 2 can be enforced through proper choice of control gains.

Assumption 3: At the instant the foot contacts the ground ($y = 0$), the ground applies an impulsive force that results in $\dot{x} = \dot{y} = 0$ instantaneously.

Assumption 3 simply implies inelastic impact.

Taking the integral over the infinitesimal period of time in which the impact occurs we have

$$\int_{t_0}^{t_0+\epsilon} \ddot{q} dt = \int_{t_0}^{t_0+\epsilon} M^{-1}(q) \left[AT - N(q, \dot{q}) + F_{ext} \right] dt \tag{3.6}$$

$$\dot{q}^+ = \dot{q}^- + M^{-1}(q) F_{ext} \tag{3.7}$$

where $\dot{q}^+$ and $\dot{q}^-$ are the right and left limits in time of $\dot{q}$. This follows from our earlier work [10]. Partitioning q according to

$$q = [x \;\; y \mid \theta]^T \tag{3.8}$$

where θ is given by

$$\theta = [\theta_1 \;\; \theta_2 \;\; \theta_3 \;\; \theta_4]^T \tag{3.9}$$

results in the corresponding partition of $M^{-1}(q)$ given by

$$M^{-1}(q) = \left[\begin{array}{c|c} (M^{-1})_{11} & (M^{-1})_{12} \\ \hline (M^{-1})_{21} & (M^{-1})_{22} \end{array} \right] \tag{3.10}$$

Solving Eq.(3.7) results in the following change in the state variables:

$$\begin{aligned} q^+ &= q^- \\ \dot{x}^+ &= 0 \\ \dot{y}^+ &= 0 \\ \dot{\theta}^+ &= \dot{\theta}^- - (M^{-1})_{21}[(M^{-1})_{11}]^{-1} \begin{bmatrix} \dot{x}^- \\ \\ \dot{y}^- \end{bmatrix} \end{aligned} \tag{3.11}$$

3.1.3 Contact Phase

During the contact phase, F_{ext} is such that $\ddot{y} = 0$.

Assumption 4: The friction force F_x is always sufficiently large such that $\ddot{x} = 0$ during the contact phase.

During the contact phase, the dynamics of the hopper is given by

$$DM(q)D^T D\ddot{q} + DN(q, \dot{q}) = DAT \tag{3.12}$$

where D is the matrix

$$D = \begin{bmatrix} 0 & 0 & 1 & 0 & 0 & 0 \\ \\ 0 & 0 & 0 & 1 & 0 & 0 \\ \\ 0 & 0 & 0 & 0 & 1 & 0 \\ \\ 0 & 0 & 0 & 0 & 0 & 1 \end{bmatrix} \tag{3.13}$$

The contact phase transitions to the flight phase when

$$F_y = 0 \qquad \dot{F}_y < 0 \tag{3.14}$$

3.2 Continuous Control

Similar to the two-mass case, in order to achieve a desired apex height we design a continuous controller that regulates the center-of-mass posistion relative to that base of the robot, point O. To control the center-of-mass, we define r to be the vector from the base of the foot to the center-of-mass of the hopper. If r_x and r_y denote the horizontal and vertical components of r, we can write

$$r = \begin{bmatrix} r_x \\ r_y \end{bmatrix} = \begin{bmatrix} f_x(q) \\ f_y(q) \end{bmatrix} \tag{3.15}$$

where $f_x(q)$ and $f_y(q)$ are given by

$$\begin{aligned} f_x(q) &= a_1 \cos(\theta_1) + a_2 \cos(\theta_1 + \theta_2) + \\ &\quad a_3 \cos(\theta_1 + \theta_2 + \theta_3) + \\ &\quad a_4 \cos(\theta_1 + \theta_2 + \theta_3 + \theta_4) \end{aligned} \tag{3.16}$$

$$\begin{aligned} f_y(q) &= a_1 \sin(\theta_1) + a_2 \sin(\theta_1 + \theta_2) + \\ &\quad a_3 \sin(\theta_1 + \theta_2 + \theta_3) + \\ &\quad a_4 \sin(\theta_1 + \theta_2 + \theta_3 + \theta_4) \end{aligned} \tag{3.17}$$

In Eq.(3.16) and (3.17), the constants have the expressions

$$\begin{aligned} a_1 &= \frac{m_1 d_1 + (m_2 + m_3 + m_4) l_1}{\overline{m}} \\ a_2 &= \frac{m_2 d_2 + (m_3 + m_4) l_2}{\overline{m}} \\ a_3 &= \frac{m_3 d_3 + m_3 l_3}{\overline{m}} \\ a_4 &= \frac{m_4 d_4}{\overline{m}} \\ \overline{m} &= m_1 + m_2 + m_3 + m_4 \end{aligned} \tag{3.18}$$

Differentiating with respect to time gives

$$\dot{r} = \begin{bmatrix} \dot{r}_x \\ \\ \dot{r}_y \end{bmatrix} = \begin{bmatrix} J_x(q) \\ \\ J_y(q) \end{bmatrix} D\dot{q} \tag{3.19}$$

where $J_x(q)$ and $J_y(q)$ are Jacobian matrices.

In addition to the control of the center of mass position r, we wish to control the angle of the first link, θ_1. To this end we define the desired equilibrium point of the system as follows:

$$(r_x, r_y, \theta_1, \dot{r}_x, \dot{r}_y, \dot{\theta}_1) = (0, y_d, \theta_d, 0, 0, 0) \tag{3.20}$$

3.2.1 Contact Phase

The continuous controller used during the contact phase is defined on the position of the center of mass, r, the angle of the foot, and the angular momentum about the foot. The center of mass positions are chosen since during contact phase, the relative center of mass position is the total center of mass position. The angular momentum is chosen as it will

determine the total angular momentum during the flight phase, and the angle of the foot is chosen to help ensure that only the point O is in contact with the ground. During the contact phase the system dynamics are described by Eq.(3.12). To transform this dynamics to normal form [20], we use the transformations in Eqs.(3.15),(3.19), and

$$\begin{aligned} \eta &= \psi_1(q) \\ \zeta_1 &= \psi_2(q,\dot{q}) = -\frac{1}{\overline{m}g} CDM(q)D^T D\dot{q} \end{aligned} \tag{3.21}$$

where the matrix C is given by

$$C = \begin{bmatrix} 1 & 0 & 0 & 0 \end{bmatrix} \tag{3.22}$$

In addition, ζ_i, $i \in [2,7]$, are defined as

$$\begin{aligned} &\zeta_2 = r_x \quad \zeta_3 = r_y - y_d \quad \zeta_4 = \theta_1 - \theta_d \\ &\zeta_5 = \dot{r}_x \quad \zeta_6 = \dot{r}_y \qquad\quad \zeta_7 = \dot{\theta}_1 \end{aligned} \tag{3.23}$$

It can be shown

$$\begin{aligned} \dot{\eta} &= \frac{\partial \psi_1(q)}{\partial q}\dot{q} = f(\eta,\zeta) \\ \dot{\zeta}_1 &= \frac{\partial \psi_2(q,\dot{q})}{\partial q}\dot{q} + \frac{\partial \psi_2(q,\dot{q})}{\dot{q}}\ddot{q} \\ &= \frac{-CD}{\overline{m}g}\left[AT - N(q,\dot{q}) + \dot{M}(q)D^T D\dot{q}\right] = \zeta_2 \end{aligned} \tag{3.24}$$

and

$$\left[\dot{\zeta}_2,\ \dot{\zeta}_3,\ \dot{\zeta}_4\right]^T = [\zeta_5,\ \zeta_6,\ \zeta_7]^T = J(q)D\dot{q} \tag{3.25}$$

$$\left[\dot{\zeta}_5,\ \dot{\zeta}_6,\ \dot{\zeta}_7\right]^T = J(q)D\ddot{q} + \dot{J}(q)D\dot{q} \tag{3.26}$$

where $J(q)$ is given by

$$J(q) = \begin{bmatrix} J_x(q) \\ J_y(q) \\ C \end{bmatrix} \tag{3.27}$$

The expression $\dot{\zeta}_1 = \zeta_2$ follows intuitively from $\overline{m}g\zeta_1$ being the angular momentum of the hopper about its foot, and $\overline{m}g\zeta_2$ being the resulting torque about the foot due to gravity.

The dynamics in Eq.(3.12) are described by Eqs.(3.24), and (3.26) in the region where the transformations in Eq.(3.21) and (3.23) are diffeomorphic. Substituting Eq.(3.12) into (3.26) gives

$$\begin{bmatrix} \dot{\zeta}_5 \\ \dot{\zeta}_6 \\ \dot{\zeta}_7 \end{bmatrix} = J(q)(DMD^T)^{-1}D\left[AT - N(q,\dot{q})\right] + \dot{J}(q)D\dot{q} \tag{3.28}$$

Define the vector of torques T to be

$$\begin{aligned} T &= [J(q)(DM(q)D^T)^{-1}DA]^{\#}[v_g \\ &\quad + J(q)(DM(q)D^T)^{-1}DN(q,\dot{q}) - \dot{J}(q)D\dot{q}] \end{aligned} \tag{3.29}$$

where $(\cdot)^{\#}$ is the right pseudo-inverse of $(\cdot)$. To prevent a singularity condition, we make

the following assumption:

Assumption 4: The Jacobean matrix $J(q)$ is full row rank over the duration that the torque T is applied.

Substituting (3.29) into (3.28) results in

$$\left[\dot{\zeta}_5,\ \dot{\zeta}_6,\ \dot{\zeta}_7\right]^T = v_g \tag{3.30}$$

We choose v_g to the be given by

$$v_g = \begin{bmatrix} -K_1\zeta_1 - K_2\zeta_2 - K_5\zeta_5 \\ -K_3\zeta_3 - \alpha K_6\zeta_6 \\ -K_4\zeta_4 - K_7\zeta_7 \end{bmatrix} \tag{3.31}$$

with α defined as

$$\alpha = \begin{cases} 1 & \zeta_6 \leq 0 \\ \nu & \zeta_6 > 0 \end{cases} \tag{3.32}$$

and the gains K_i chosen such that $K_i > 0\ \forall i$ and

$$K_6 < 2\sqrt{K_3} \tag{3.33}$$

This ensures asymptotic convergence of trajectories to the manifold

$$\mathcal{M} = \{\zeta \in \mathbb{R}^7 | (\zeta_1, \zeta_2, \zeta_4, \zeta_5, \zeta_7) = (0, 0, 0, 0, 0)\} \tag{3.34}$$

On $\mathcal{M}$, the trajectories of the system obey

$$\begin{bmatrix} \dot{\zeta}_3 \\ \dot{\zeta}_6 \end{bmatrix} = \begin{bmatrix} 0 & 1 \\ -K_3 & -\alpha K_6 \end{bmatrix} \begin{bmatrix} \zeta_3 \\ \zeta_6 \end{bmatrix} \tag{3.35}$$

which represents a "mass spring damper" whose damping is positive or negative based on the value of ν. By modulating ν we will increase or decrease the energy of the system and achieve apex height control.

3.2.2 Flight Phase

During the flight phase, the position of the foot relative to the center of mass is controlled in order to achieve a desired foot placement at the time of touchdown. In this phase the system has the additional dynamics of x, $\dot{x}$, y, and $\dot{y}$, which were not present in the contact phase. We define the states as.

$$\begin{aligned} d &= x + r_x, \quad h = y + r_y \\ \dot{d} &= \dot{x} + \dot{r}_x, \quad \dot{h} = \dot{y} + \dot{r}_y \end{aligned} \tag{3.36}$$

where d and h represent the horizontal and vertical component of the center of mass in the inertial frame of reference. Using Eq.(3.2) we can show

$$\ddot{d} = 0, \qquad \ddot{h} = -g \tag{3.37}$$

Additionally, the angular momentum of the system about its center of mass is conserved. The angular momentum about the center of mass is given by

$$H_c = \sum_{i=1}^{4} \left[r_i \times m_i \dot{r}_i + I_i \sum_{j=1}^{i} \dot{\theta}_j \right] \tag{3.38}$$

Substituting Eqs.(3.21) and (3.23) into (3.38) gives

$$H_c = -\overline{m}[g\zeta_1 + (\zeta_3 + y_d)\zeta_5 - \zeta_2\zeta_6] \tag{3.39}$$

sovling Eq.(3.39) for ζ_1 gives

$$\zeta_1 = \frac{1}{\overline{m}g} \left[\overline{m}\zeta_2\zeta_6 - \overline{m}(\zeta_3 + y_d)\zeta_5 - H_c \right] \tag{3.40}$$

This shows ζ_1 is related to ζ_2, ζ_3, ζ_5, and ζ_6 via an algebraic relationship. The dynamics of ζ_2, ζ_3, and ζ_4 are the same as in Eq.(3.25), whereas the dynamics of ζ_5, ζ_6, and ζ_7 can be obtained by substituting Eq.(3.2) into Eq.(3.26):

$$\begin{bmatrix} \dot{\zeta}_5 \\ \dot{\zeta}_6 \\ \dot{\zeta}_7 \end{bmatrix} = J(q)DM^{-1} \left[AT - N(q, \dot{q}) \right] + \dot{J}(q)D\dot{q} \tag{3.41}$$

Defining the vector of torques T to be

$$\begin{aligned} T &= [J(q)DM^{-1}(q)A]^{\#}[v_f \\ &\quad + J(q)DM^{-1}(q)N(q, \dot{q}) - \dot{J}(q)D\dot{q}] \end{aligned} \tag{3.42}$$

results in

$$\left[\dot{\zeta}_5,\ \dot{\zeta}_6,\ \dot{\zeta}_7\right]^T = v_f \tag{3.43}$$

We choose v_f as follows:

$$v_f = \begin{bmatrix} -K_2\zeta_2 - K_5\zeta_5 \\ -K_3\zeta_3 - K_6\zeta_6 \\ -K_4\zeta_4 - K_7\zeta_7 \end{bmatrix} \tag{3.44}$$

where $K_i > 0\ \forall i \in [2,\ 7]$. This guarantees that the variables $\zeta_i\ i \in [2,\ 7]$ will asymptotically converge to zero. Additionally, if $H_c = 0$, ζ_1 will asymptotically converge to zero. Since the angular moment H_c cannot be controlled in the flight phase, our objective is to bring it to zero during the contact phase.

3.2.3 Hybrid Dynamics of Closed-Loop System

The hybrid dynamics of the system over one hop is summarized as follows:

The system begins with the Flight Phase. The dynamics during flight phase is described by

$$\begin{bmatrix} \ddot{d} \\ \ddot{h} \\ \dot{\eta} \end{bmatrix} = \begin{bmatrix} 0 \\ -g \\ f(\eta,\zeta) \end{bmatrix}, \qquad \begin{bmatrix} \dot{\zeta}_2 \\ \dot{\zeta}_3 \\ \dot{\zeta}_4 \end{bmatrix} = \begin{bmatrix} \zeta_5 \\ \zeta_6 \\ \zeta_7 \end{bmatrix} \tag{3.45}$$

$$\begin{bmatrix} \dot{\zeta}_5 \\ \dot{\zeta}_6 \\ \dot{\zeta}_7 \end{bmatrix} = \begin{bmatrix} -K_2\zeta_2 - K_5\zeta_5 \\ -K_3(\zeta_3 - y_d) - K_6\zeta_6 \\ -K_4(\zeta_4 - \theta_d) - K_7\zeta_7 \end{bmatrix} \tag{3.46}$$

and the non-holonmic constraint given by Eq.(3.40) for ζ_1.

Following the flight phase the system undergoes Impact. The hopper makes contact with

the ground when $y = 0$ or $h - \zeta_3 - y_d = 0$. The impulse due to impact is given by Eq.(3.11).

Following the Impact, the system is in Contact Phase. From Eqs.(3.24), (3.26), (3.30) and (3.31), and $\ddot{x} = \ddot{y} = 0$ the dynamics during contact phase are given by

$$\begin{bmatrix} \dot{\eta} \\ \dot{\zeta}_1 \\ \dot{\zeta}_2 \\ \dot{\zeta}_3 \\ \dot{\zeta}_4 \end{bmatrix} = \begin{bmatrix} f(\eta, \zeta) \\ \zeta_2 \\ \zeta_5 \\ \zeta_6 \\ \zeta_7 \end{bmatrix}, \qquad \begin{bmatrix} \dot{\zeta}_5 \\ \dot{\zeta}_6 \\ \dot{\zeta}_7 \end{bmatrix} = \begin{bmatrix} -K_1\zeta_1 - K_2\zeta_2 - K_5\zeta_5 \\ -K_3(\zeta_3 - y_d) - \alpha K_6\zeta_6 \\ -K_4(\zeta_4 - \theta_d) - K_7\zeta_7 \end{bmatrix} \tag{3.47}$$

where

$$\alpha = \begin{cases} 1 & \zeta_6 \leq 0 \\ \nu & \zeta_6 > 0 \end{cases} \tag{3.48}$$

and the states h and $\dot{d}$ are given by

$$h \equiv \zeta_3 + y_d, \qquad \dot{d} \equiv \zeta_5 \tag{3.49}$$

The contact phase ends at the instant F_y in Eq.(3.5) is equal to 0, that is

$$F_y = \overline{m}\dot{\zeta}_6 + \overline{m}g = 0 \Rightarrow \dot{\zeta}_6 = -g \tag{3.50}$$

3.3 Periodic Behavior

Hopping is described by consecutive sequences of flight phase, impact, and contact phase. To describe a single hop, we define the state χ

$$\chi \in \Omega, \qquad \Omega = \{(\theta, \dot{\theta}) \mid \dot{\zeta}_6(\theta, \dot{\theta}) + g = 0\} \tag{3.51}$$

which define the configuration of the hopper at the time of transition from the contact to the flight phase. The configuration χ does not include d since the objective of this paper is to control only the height. The first return map between the kth hop and the $(k+1)$th hop is defined as

$$\chi(k+1) = P(\chi(k)) \tag{3.52}$$

where $P(\chi(k))$ is the solution of the closed-loop hybrid dynamics.

3.3.1 Period One Orbits

For a period-one orbit [9] we have

$$\chi(k) - P(\chi(k)) = 0 \tag{3.53}$$

Let χ^* to be any value of χ that satisfies Eq.(3.53). Note that χ lies in a 7 embedded manifold of $\mathbb{R}^8$. Let V to be the matrix of linearly independent unit vectors

$$V = [v_1, v_2, \ldots v_7] \qquad v_i \in \mathbb{R}^8,\ |v_i| = 1,\ i \in [1, 7] \tag{3.54}$$

where

$$\text{span}(V) = \Omega \tag{3.55}$$

Linearization of Eq.(3.52) about the periodic point χ^* gives

$$\chi(k+1) \approx P(\chi^*) + \sum_{i=1}^{7} \left[\frac{\partial P(\chi)}{\partial v_i} v_i^T |_{\chi=\chi^*} (\chi(k) - \chi^*) \right] \tag{3.56}$$

where $\partial P(\chi)/\partial v_i$ is given by

$$\frac{\partial P(\chi)}{\partial v_i} = \lim_{h \to 0} \frac{P(\chi + h v_i) - P(\chi)}{h} \tag{3.57}$$

It follows that Eq.(3.56) is asymptotically stable iff

$$\rho \left(\sum_{i=1}^{7} \left[\frac{\partial P(\chi)}{\partial v_i} v_i^T |_{\chi=\chi^*} \right] \right) < 1 \tag{3.58}$$

where $\rho(\cdot)$ is the spectral radius.

3.3.2 Chaos Control

A periodic orbit defined by χ^* may not be stable for a given set of system parameters. However, we note that $P(\chi)$ is dependent on the variable ν. By defining ν^* to be the value of ν that satisfies Eq.(3.53) for $\chi = \chi^*$, we will vary the value of ν to ensure asymptotic stability of χ^*.

To design the input $\nu(k)$, first define the vector $\overline{v}$ as

$$\overline{v} = \begin{bmatrix} a \\ \\ b \end{bmatrix} \qquad |\overline{v}| = 1,\ a \in \mathbb{R}^8,\ b \in \mathbb{R} - \{0\} \tag{3.59}$$

where a satisfies Eq.(3.50). Defining the error E and the input u as

$$\begin{aligned} E(k) &= \chi(k) - \chi^* \\ u(k) &= \nu(k) - \nu^* \end{aligned} \tag{3.60}$$

we have the linearized equation of Eqn. (3.53):

$$E(k+1) = AE(k) + Bu(k) \tag{3.61}$$

where A and B are given by

$$\begin{aligned} A &= \sum_{i=1}^{7} \left[\frac{\partial P(\chi)}{\partial v_i} v_i^T \right] + \frac{\partial P(\chi(k))}{\partial \overline{v}} a^T \\ B &= \frac{\partial P(\chi(k))}{\partial \overline{v}} b \end{aligned} \tag{3.62}$$

and where the directional derivatives $\partial P(\chi)/\partial v_i$ and $\partial P(\chi)/\partial \overline{v}$ are evaluated at (χ^*, ν^*). For asymptotic stability, $u(k)$ is designed as

$$u(k) = GE(k) \tag{3.63}$$

where G is chosen such that

$$\rho(A + BG) < 1 \tag{3.64}$$

3.4 Simulations

For the four-link hopper, the masses are assumed to be

$$m_1 = 2.5\ kg,\ m_2 = 5\ kg,\ m_3 = 10\ kg,\ m_4 = 20\ kg \tag{3.65}$$

The length of the links of the hopper are assumed to be

$$l_1 = 0.1\ m, \quad l_2 = l_3 = l_4 = 0.3\ m \tag{3.66}$$

and the distance to the center of mass of each link - see Fig.3.1 are assumed to be

$$d_1 = 0.05\ m, \quad d_2 = d_3 = d_4 = 0.15\ m \tag{3.67}$$

The moment of inertia of each link is computed as

$$I_i = \frac{1}{12} m_i l_i^2 \qquad \forall i \in [1, 4] \tag{3.68}$$

The gains used for the continuous control are

$$\begin{aligned} &K_1 = 12000 \quad K_2 = 8000 \quad K_3 = 300 \quad K_4 = 300 \\ &K_5 = 120 \qquad K_6 = 10 \qquad K_7 = 8 \end{aligned} \tag{3.69}$$

and the set points y_d and θ_d for the continuous control are

$$y_d = 0.4967\ m \qquad \theta_d = \frac{\pi}{2} - 0.1 \tag{3.70}$$

The value of y_d is 0.14 m below the maximum height of the center of mass relative to the foot.

We choose the desired apex height of the center of mass to be 0.65 meters and compute the periodic point, (χ^*, ν^*) to be given by

$$\begin{array}{lll} \chi_1^* = 1.579 & \chi_2^* = -0.407 & \chi_3^* = 1.135 \\ \chi_4^* = -1.178 & \chi_5^* = -6.696 & \chi_6^* = 11.659 \\ \chi_7^* = -10.360 & \chi_8^* = 8.960 & \nu^* = -0.607 \end{array} \tag{3.71}$$

with all values given in rad and rad/s where appropriate. The periodic point is computed numerically via a regression algorithm. The algorithm uses an initial guess for the periodic values (χ^*, ν^*). The algorithm restricts the guesses to the manifold which satisfy the desired apex height. It then uses a regressive minimization algorithm to minimize the difference between the guessed lift-off values and the values for the resulting values from letting the system progress for a single hop.

The stabilizing control gains G for the periodic point in Eq.(5.73) are by solving the discrete LQR problem:

$$\begin{array}{lll} G_1 = -0.023 & G_2 = 0.025 & G_3 = -0.005 \\ G_4 = 0.011 & G_5 = -0.051 & G_6 = -0.030 \\ G_7 = 0.005 & G_8 = -0.027 & \end{array} \tag{3.72}$$

We choose the initial configuration of the system is assumed to be

$$\begin{aligned}(x(0), \dot{x}(0), y(0), \dot{y}(0)) &= (0.00, 0.00, 0.03, 0.00) \\ \theta(0) &= [1.65,\ -0.50,\ 1.07,\ -0.94]^T \\ \dot{\theta}(0) &= [0.00,\ 0.00,\ 0.00,\ 0.00] \end{aligned} \tag{3.73}$$

where the units are in meters, rad, and rad/sec. These initial conditions were chosen such that the center of mass of the hopper lies vertically above the point of support. The initial value of the discrete control input is chosen to be

$$u(0) = 0 \Rightarrow \nu(0) = \nu^* \tag{3.74}$$

Figure 3.2 shows the height of the center of mass as a function of time. It can be seen that the center of mass converges to the desired height in approximately 4 hops. Figure 3.3 displays the inputs torques τ_1, τ_2, and τ_3. The sharp peaks indicate the discontinuous jumps in the torques immediately following impact.

From the simulations we see the efficacy of the control method as applied to a four-linked hopping robot. We note that all results of this chapter are for robots that are interacting with a rigid ground, namely ground surfaces whose rigidity is sufficiently high as to consider them to not deform under the applied forces of the robot. However, it behooves us to investigate the motion of hopping robots when the their contact is an elastic surface instead of a rigid one, namely a surface which does deform under the mass of the robot. To this end, we will investigate both a two mass hopping robot, and a three-link hopping robot when interacting with and elastic ground.

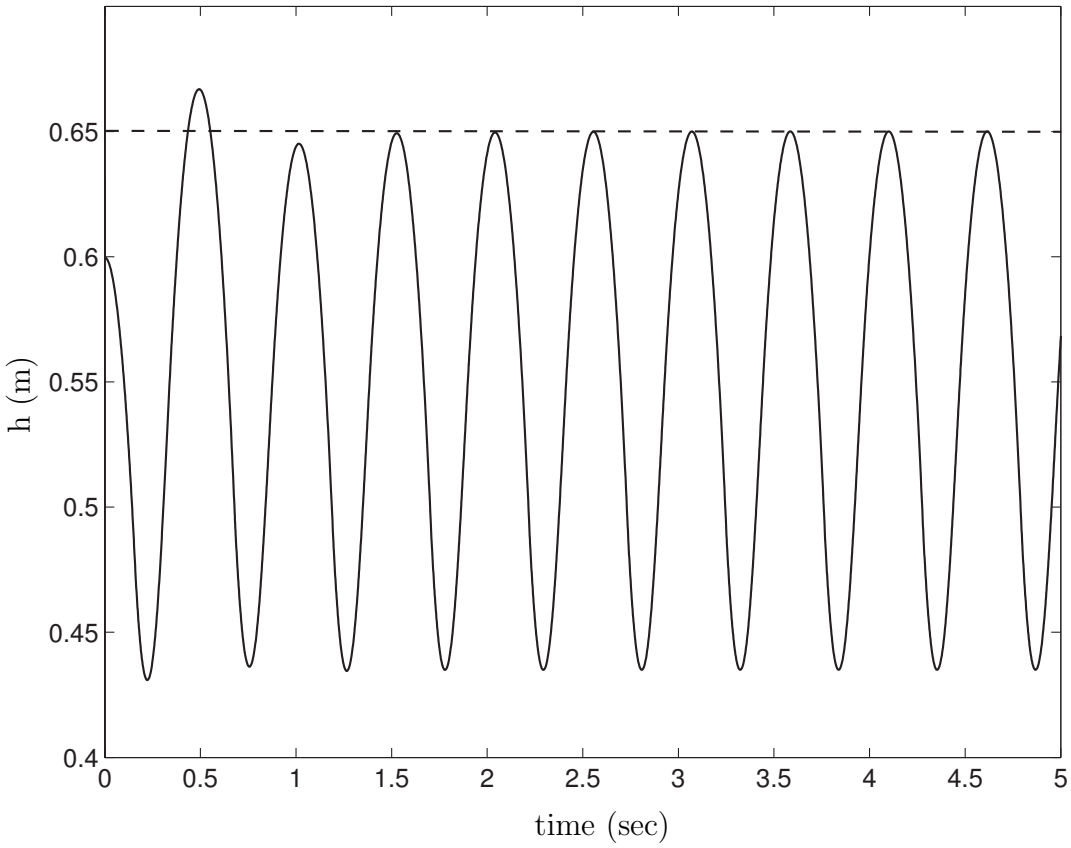

Figure 3.2: Center of mass height above the ground for the four-link hopper

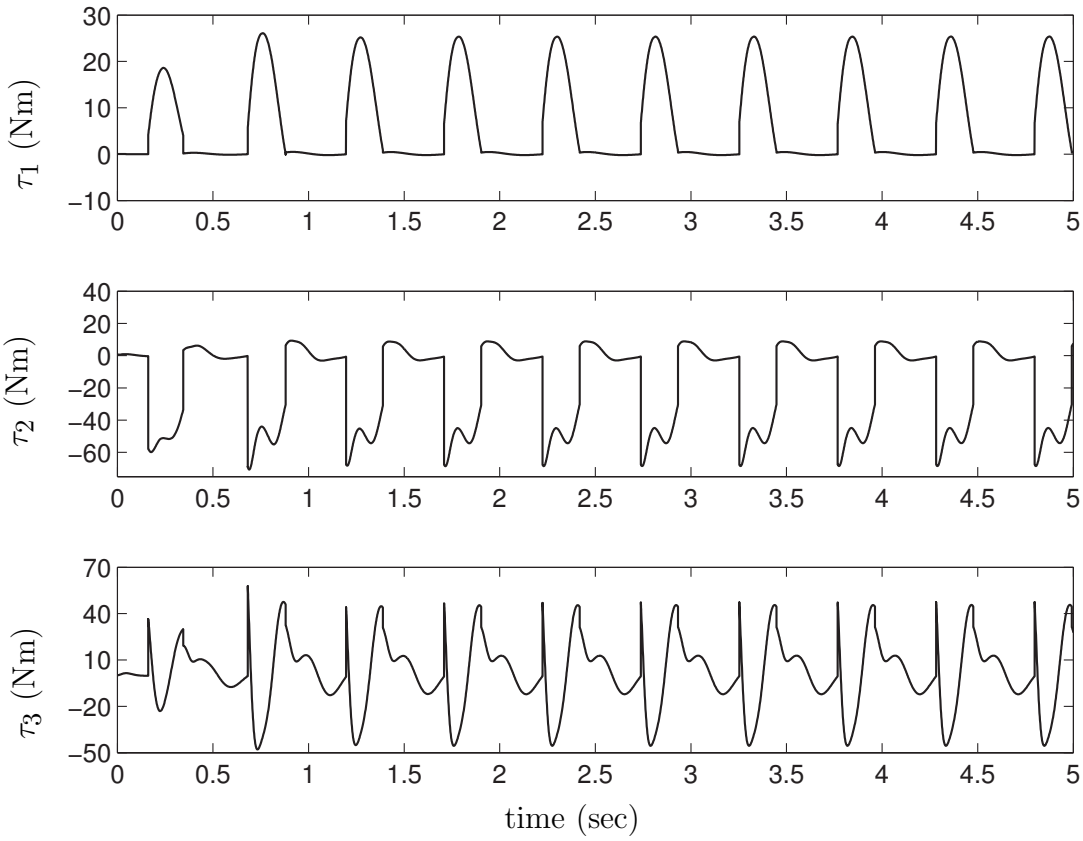

Figure 3.3: Input torques for the four-link hopper

Chapter 4

Two-Mass Hopping Robot on an Elastic Foundation

Unlike with the rigid ground interaction, and elastic ground interaction assumes that the ground does deform under the mass of the robot. For this purpose we model the interaction of the elastic ground as an interaction with a massless spring. Similarly with the rigid foundation, we begin with the analysis of a simplified two-mass hopping robot before moving on to the analysis of a three-link hopping robot.

As with Chapter 2, We start the analysis of a linked hopping robot on an elastic foundation with the analysis and control of a simplified 2 mass robot hopping on an elastic foundation. We begin with a discussion of the dynamics of the two mass system hopping on an elastic foundation and the discuss the necessity of changing the control algorithm from the rigid foundation case. We then discuss a hybrid control algorithm which uses backstepping [19] to stabilize the dynamics of the robot in the flight and contact phases. The periodic nature of the hybrid dynamic system is then analyzed using a Poincare map [9] and the OGY[1] method of chaos control [29] is used to adjust a parameter discretely and converge to the desired apex height. The results in the chapter follow the results presented by Mathis and Mukherjee [23].

[1] A method introduced by Ott, Grebogi and Yorke for achieving stabilization of a periodic orbit [29].

4.1 Dynamics

4.1.1 System Description

Consider the two-mass robot in Fig.4.1 (a), which is hopping on a massless elastic foundation of stiffness K_{ext}. It is comprised of an upper mass m_1 and a lower mass m_2. The upper and lower masses are connected by a prismatic joint. The force applied by the actuator in the prismatic joint on the two masses is denoted by F; it is assumed that this force can be actively controlled. The positions of the center-of-mass of m_1 and m_2 from the datum are denoted by x_1 and x_2. The position of the center-of-mass of m_1 relative to that of m_2 is denoted by y and the height of the center-of-mass of m_2 from the base of m_2 is denoted by ℓ. The force of interaction between the lower mass and the elastic foundation is denoted by F_{ext}.

4.1.2 Flight Phase

During the flight phase, the following conditions hold:

$$x_2 > \ell \qquad F_{\text{ext}} = 0 \tag{4.1}$$

The equations of motion of the robot are as follows:

$$\ddot{x}_1 = -g + \frac{F}{m_1} \qquad \ddot{x}_2 = -g - \frac{F}{m_2} \tag{4.2}$$

Using the relative displacement $y \triangleq (x_1 - x_2)$ to replace x_1, an alternate form of the equations

of motion are

$$\ddot{y} = \left[\frac{m_{\rm t}}{m_1 m_2}\right] F \qquad \ddot{x}_2 = -g - \frac{F}{m_2} \tag{4.3}$$

where the total mass of the system is

$$m_{\rm t} \triangleq (m_1 + m_2) \tag{4.4}$$

4.1.3 Contact Phase

For the contact phase, we make the following assumptions:

Assumption 1: The elastic foundation has no mass and behaves like a spring.

Assumption 2: The force exerted by the elastic foundation on mass m_2 is non-negative, *i.e.*,

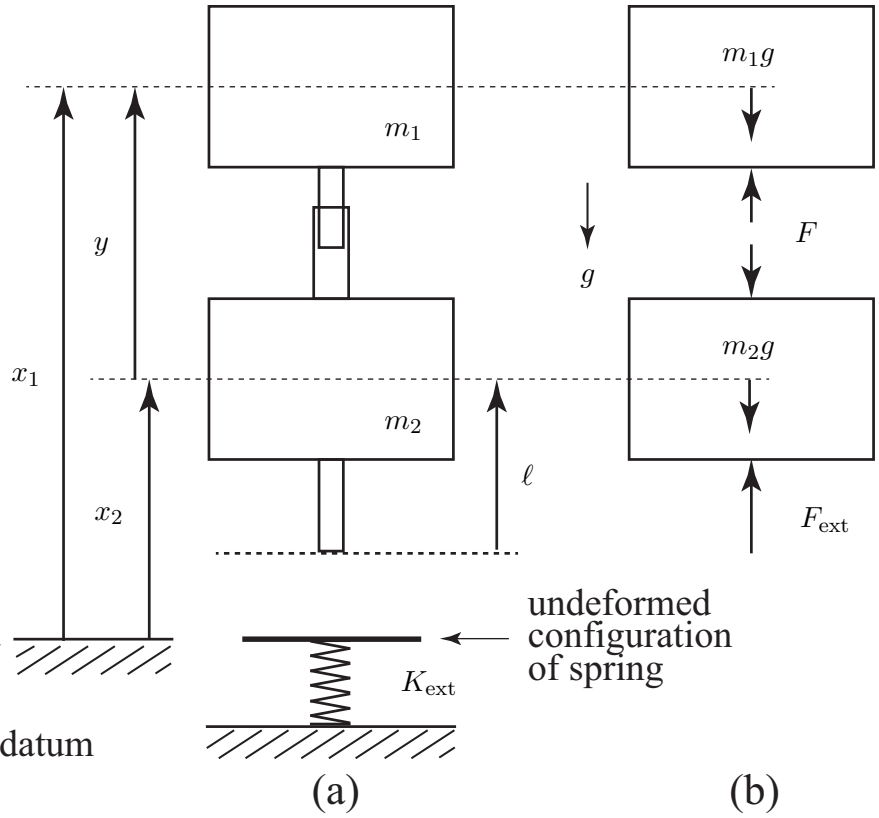

Figure 4.1: (a) Two-mass robot hopping on an elastic foundation (b) free-body diagrams of the two masses at an instant when the lower mass is in contact with the elastic foundation.

$F_{\text{ext}} \geq 0$.

From the free-body diagrams, the equations of motion of the robot can be obtained as follows:

$$\ddot{x}_1 = -g + \frac{F}{m_1} \qquad \ddot{x}_2 = -g + \frac{(F_{\text{ext}} - F)}{m_2} \tag{4.5}$$

In y and x_2 coordinates, these equations can be written as

$$\ddot{y} = \left[\frac{m_{\text{t}}}{m_1 m_2}\right] F - \frac{F_{\text{ext}}}{m_2} \qquad \ddot{x}_2 = -g + \frac{(F_{\text{ext}} - F)}{m_2} \tag{4.6}$$

In (4.5) and (4.6), F_{ext} is given by the expression

$$F_{\text{ext}} = -K_{\text{ext}}(x_2 - \ell) \tag{4.7}$$

4.1.4 Apex Height

If z denotes the height of the center-of-mass of the hopping robot, we have

$$z = \frac{m_1 x_1 + m_2 x_2}{m_1 + m_2} = x_2 + m_{\text{f}}\, y, \quad m_{\text{f}} \triangleq (m_1/m_{\text{t}}) \tag{4.8}$$

For each flight phase, the apex height is defined as the maximum value of z, and is denoted by h.

4.2 Motivation for Different Control Strategy

From Chapter 2.2 we have the dynamics of the closed loop system are given by:

$$\begin{aligned} \ddot{x} &= K[m_f y - r_d] + D m_f \dot{y} - g + \frac{\lambda}{m_2} F_{ext} \\ \ddot{y} &= -K \left[y - \frac{1}{m_f} r_d \right] - \nu D \dot{y} \end{aligned} \tag{4.9}$$

The convergence of the algorithm relies on the use of the gradient of the trajectories with respect to gain ν around the periodic point. This works in the case of the rigid foundation because of the change in momentum due to the impulse during ground impact ensures that the periodic orbit does not satisfy $\dot{y} \equiv 0$.

However, the external force creates a conservative system in the elastic foundation. This produces the periodic orbit

$$\begin{aligned} \ddot{x} &= -g + \frac{\lambda}{m_2} F_{ext} \\ \ddot{y} &\equiv \dot{y} \equiv 0 \end{aligned} \tag{4.10}$$

We not that this periodic trajectory sets the apex height based on the initial condition and is independent of the value ν. Furthermore, this From this we see that the gradient of the periodic trajectory with respect to ν is 0 since $\dot{y} \equiv 0$ during these periodic points. This means that the previous method will not work for these points since the control has no effect at any periodic orbit. Therefore, we must utilize a new closed loop method which utilizes parameter variations which have non-zero gradient at the periodic orbit.

4.3 Hybrid Control Strategy

4.3.1 Control Problem Definition

We first define r to be the height of the center-of-mass of the robot relative to that of the lower mass m_2. Using (4.8), it can be shown

$$r \triangleq (z - x_2) = m_{\mathrm{f}}\, y \tag{4.11}$$

Next, we define e as

$$e = (r - r_{\mathrm{d}}) \tag{4.12}$$

where $r_{\mathrm{d}} > 0$ is some desired value of r. From (4.11) and (4.12) it can be verified that $e \equiv 0 \rightarrow \dot{e} \equiv 0 \rightarrow \dot{y} \equiv 0$, which implies no relative motion between the two masses.

If there is no relative motion of the masses, the total energy of the system is the sum of the kinetic and potential energies of the center-of-mass plus the potential energy stored in the elastic foundation. The potential energy of the center-of-mass is defined relative to the datum $z = z_{\mathrm{d}}$, where

$$z_{\mathrm{d}} \triangleq z\,|_{(x_2=\ell, r=r_{\mathrm{d}})} = (r_{\mathrm{d}} + \ell)$$

In the absence of relative motion of the masses, the total energy can be written as

$$E = m_{\mathrm{t}} \left[\frac{1}{2}\dot{z}^2 + g(z - z_{\mathrm{d}})\right] + \frac{1}{2}\lambda K_{\mathrm{ext}}\,(z - z_{\mathrm{d}})^2 \tag{4.13}$$

where

$$\lambda = \begin{cases} 0 & : \quad x_2 \geq \ell - \text{ Flight Phase} \\ 1 & : \quad x_2 < \ell - \text{ Contact Phase} \end{cases} \tag{4.14}$$

The second term on the right-hand side of (4.13) represents the potential energy stored in the spring when the two masses are in their nominal position relative to one another. For the robot to reach its desired apex height h_{d}, the total energy should be equal to

$$E \equiv E_{\mathrm{des}} = m_{\mathrm{t}}\, g(h_{\mathrm{d}} - z_{\mathrm{d}}) \tag{4.15}$$

in addition to $e \equiv 0$. The desired equilibrium configuration is therefore given by

$$(E - E_{\mathrm{des}}, e, \dot{e}) = (0, 0, 0) \tag{4.16}$$

4.3.2 Continuous Controller Design for Stabilization in Flight and Contact Phases

4.3.3 Feedback Linearization

For the convenience of control design, we rewrite the dynamics of the hybrid system in terms of variables z and e. Using (4.4), (4.6), (4.7), (4.8), (4.11) and (4.12), the hybrid dynamics of the robot can be described by the relations

$$\ddot{z} = -g - \lambda \frac{1}{m_{\mathrm{t}}} K_{\mathrm{ext}}(x_2 - \ell) \tag{4.17}$$

$$\ddot{e} = \frac{1}{m_2}\left[F - \lambda\, m_{\mathrm{f}} F_{\mathrm{ext}}\right] \tag{4.18}$$

where λ is defined in (4.14). The following choice of the control input F

$$F = \lambda\, m_{\mathrm{f}} F_{\mathrm{ext}} + m_2 v \tag{4.19a}$$

$$= -\lambda\, m_{\mathrm{f}} K_{\mathrm{ext}}(x_2 - \ell) + m_2 v \tag{4.19b}$$

results in the hybrid dynamics

$$\ddot{z} = -g - \lambda \frac{1}{m_{\mathrm{t}}} K_{\mathrm{ext}}(x_2 - \ell) \tag{4.20}$$

$$\ddot{e} = v \tag{4.21}$$

where v is the new control input. Note that the control input F can be chosen according to (4.19a) or (4.19b) depending on whether the external force F_{ext} or the position of the lower mass x_2 is available for measurement.

4.3.4 Backstepping

With the objective of stabilizing the equilibrium in (4.16), we first define the Lyapunov function candidate

$$V_1 = \frac{1}{2} k_e \left(E - E_{\mathrm{des}}\right)^2 \tag{4.22}$$

where k_e is a positive constant. It should be noted that V_1 is a function of λ (since E is a function of λ) but it is continuously differentiable in both the flight phase and contact phase. The Lyapunov function candidates introduced below be used for our analysis of stability in both phases and therefore we treat λ as constant and do not make any distinction between the two phases in our derivation. Using (4.12), (4.20), (4.13), and (4.22), $\dot{V}_1$ can be computed

as

$$\begin{aligned}\dot{V}_1 &= k_e \left(E - E_{\text{des}}\right) \dot{E} \\ &= k_e \left(E - E_{\text{des}}\right) \dot{z} \left[m_{\text{t}}(\ddot{z} + g) + \lambda K_{\text{ext}}(z - z_{\text{d}})\right] \\ &= k_e \left(E - E_{\text{des}}\right) \lambda K_{\text{ext}} \dot{z} e \end{aligned} \tag{4.23}$$

By choosing

$$e = \left\{-\lambda k_e \left(E - E_{\text{des}}\right) \dot{z}\right\} \triangleq \phi_1 \tag{4.24}$$

we can make $\dot{V}_1$ negative semi-definite; therefore, integrator backstepping is introduced by defining the new variable

$$q_1 = e + \lambda k_e \left(E - E_{\text{des}}\right) \dot{z} = (e - \phi_1) \tag{4.25}$$

and the composite Lyapunov function

$$V_2 = V_1 + \frac{1}{2} q_1^2 = \frac{1}{2} k_e \left(E - E_{\text{des}}\right)^2 + \frac{1}{2} q_1^2 \tag{4.26}$$

where where k_1 is a positive constant. Differentiating V_2 and substituting (4.23) and (4.25), we get

$$\begin{aligned}\dot{V}_2 &= k_e \left(E - E_{\text{des}}\right) \lambda K_{\text{ext}} \dot{z} e + q_1 \dot{q}_1 \\ &= k_e \left(E - E_{\text{des}}\right) \lambda K_{\text{ext}} \dot{z} \left[q_1 - \lambda k_e \left(E - E_{\text{des}}\right) \dot{z}\right] + q_1 \dot{q}_1 \\ &= -\lambda^2 k_e^2 K_{\text{ext}} \left(E - E_{\text{des}}\right)^2 \dot{z}^2 \\ &\qquad + q_1 \left[\dot{q}_1 + k_e \left(E - E_{\text{des}}\right) \lambda K_{\text{ext}} \dot{z}\right] \end{aligned} \tag{4.27}$$

By choosing $k_1 > 0$ and

$$\dot{q}_1 = \{-\lambda k_e K_{\text{ext}} (E - E_{\text{des}}) \dot{z} - k_1 q_1\} \triangleq \phi_2 \tag{4.28}$$

we can make $\dot{V}_2$ negative semi-definite. We introduce integrator backstepping again by defining the new variable

$$q_2 = (\dot{q}_1 - \phi_2) \tag{4.29}$$

and the composite Lyapunov function

$$\begin{aligned} V_3 &= V_2 + \frac{1}{2} q_2^2 \\ &= \frac{1}{2} k_e (E - E_{\text{des}})^2 + \frac{1}{2} q_1^2 + \frac{1}{2} q_2^2 \end{aligned} \tag{4.30}$$

Differentiating V_3 and substituting (4.27) and (4.29), we get

$$\begin{aligned} \dot{V}_3 &= -\lambda^2 k_e^2 K_{\text{ext}} (E - E_{\text{des}})^2 \dot{z}^2 \\ &\quad + q_1 [\dot{q}_1 + \lambda k_e K_{\text{ext}} (E - E_{\text{des}}) \dot{z}] + q_2 \dot{q}_2 \\ &= -\lambda^2 k_e^2 K_{\text{ext}} (E - E_{\text{des}})^2 \dot{z}^2 \\ &\quad + q_1 [\dot{q}_1 - \phi_2 - k_1 q_1] + (\dot{q}_1 - \phi_2)(\ddot{q}_1 - \dot{\phi}_2) \\ &= -\lambda^2 k_e^2 K_{\text{ext}} (E - E_{\text{des}})^2 \dot{z}^2 - k_1 q_1^2 \\ &\quad + q_2 \left[\ddot{q}_1 - \dot{\phi}_2 + q_1 \right] \end{aligned} \tag{4.31}$$

Our choice of

$$\ddot{q}_1 = \dot{\phi}_2 - q_1 - k_2 q_2, \qquad k_2 > 0 \tag{4.32}$$

results in a negative semi-definite $\dot{V}_3$ and yields the controller

$$v = \ddot{\phi}_1 + \dot{\phi}_2 - q_1 - k_2 q_2 \tag{4.33}$$

The above equation was obtained from (4.32) by substituting (4.21) and (4.25). From the definition of ϕ_1 in (4.24), it is clear that $\ddot{\phi}_1$ will involve the third derivative of z. This is not a problem since the third derivative of z can be computed easily from (4.20) as

$$\dddot{z} = -\lambda \frac{1}{m_{\mathrm{t}}} K_{\mathrm{ext}} \dot{x}_2 \tag{4.34}$$

The complete control law is given by (4.33) and (4.19a) or (4.19b).

4.3.5 Stability Analysis

Using (4.11), (4.12), (4.13), (4.17), (4.25) and (4.29) it can be shown that

$$(E - E_{\mathrm{des}}, e, \dot{e}) = (0, 0, 0) \;\Leftrightarrow\; (E - E_{\mathrm{des}}, q_1, q_2) = (0, 0, 0)$$

Therefore, V_3 in (4.30) is a candidate Lyapunov function for investigating the stability of the equilibrium in (4.16).

In the flight phase, $\lambda = 0$. For the control law given by (4.33), the derivative of the

Lyapunov function in (4.31) can be shown to be

$$\dot{V}_3 = -k_1 q_1^2 - k_2 q_2^2 \leq 0 \tag{4.35}$$

Therefore, $(E - E_{\text{des}}, q_1, q_2) = (0, 0, 0)$ is stable.

In the contact phase, $\lambda = 1$. For the control law given by (4.33), the derivative of the Lyapunov function in (4.31) is

$$\dot{V}_3 = -k_e K_{\text{ext}} \left(E - E_{\text{des}}\right)^2 \dot{z}^2 - k_1 q_1^2 - k_2 q_2^2 \leq 0 \tag{4.36}$$

Therefore, $(E - E_{\text{des}}, q_1, q_2) = (0, 0, 0)$ is stable.

Remark 1. The stability of $(E - E_{\text{des}}, q_1, q_2) = (0, 0, 0)$ in the flight and contact phases do not guarantee its stability for the hybrid dynamics.

4.3.6 Discrete Controller for Stabilization of Hybrid Dynamics

To investigate the stability of the hybrid dynamic system, we use a Poincare map with the Poincare section defined by the instant when the system transitions from the contact phase to the flight phase. The Poincare section is defined as

$$\begin{aligned} \mathcal{Z} &\coloneqq \left\{ X \in \mathbb{R}^3 | \; x_2 = \ell, \; \dot{x}_2 > 0 \right\} \\ \Rightarrow \; \mathcal{Z} &\coloneqq \left\{ X \in \mathbb{R}^3 | \; z = e + z_d, \; \dot{z} > \dot{e} \right\} \end{aligned} \tag{4.37}$$

where X is defined as

$$X = \begin{bmatrix} \dot{z} & e & \dot{e} \end{bmatrix}^T$$

To use the same set of variables used in the Lyapunov analysis, namely, $(E - E_{\text{des}})$, q_1 and q_2, we define the Poincare section using the coordinates Ψ, where Ψ is defined by the coordinate transformation $H(\cdot) : \mathbb{R}^3 \Rightarrow \mathbb{R}^3$, as follows

$$\Psi = \begin{bmatrix} (E - E_{\text{des}}) & q_1 & q_2 \end{bmatrix}^T = H(X) \tag{4.38}$$

It can be shown that the map $H(\cdot)$ is a local homeomorphism and therefore locally topologically conjugate [9]; this implies that the stability of the Poincare maps in Ψ and X coordinates are equivalent. The Poincare map $P(\Psi)$ and the sequence of points $\Psi_k \in H(\mathcal{Z})$ satisfy

$$\Psi_{k+1} = P(\Psi_k), \quad P(\Psi) : H(\mathcal{Z}) \mapsto H(\mathcal{Z}) \tag{4.39}$$

with periodic point Ψ^* defined as

$$\Psi^* = P(\Psi^*) \tag{4.40}$$

For the elastic foundation, the periodic point which achieves the desired apex height is given by

$$\Psi^* = \begin{bmatrix} 0 & 0 & 0 \end{bmatrix}^T \tag{4.41}$$

We define the error state η_k as

$$\eta_k = (\Psi_k - \Psi^*) = \Psi_k$$

By linearizing the Poincare map about Ψ^*, we have the approximate discrete dynamics given by

$$\eta_{k+1} = A\,\eta_k \qquad A \triangleq \left.\frac{dP(\Psi)}{d\Psi}\right|_{\Psi=\Psi^*} \tag{4.42}$$

The periodic point will be asymptotically stable if and only if

$$\rho(A) < 1 \tag{4.43}$$

where $\rho(A)$ is the spectral radius of A. Since the condition in (4.43) may not be satisfied, we design a discrete controller to stabilize the closed-loop system; the discrete controller is discussed next.

To design the discrete controller, we redefine Ψ as follows

$$\begin{aligned} \Psi &= \Phi + \begin{bmatrix} 1 & 0 & 0 \end{bmatrix}^T u \\ \Phi &\triangleq \begin{bmatrix} (E - E_{\mathrm{d}}) & q_1 & q_2 \end{bmatrix}^T, \quad u \triangleq (E_{\mathrm{d}} - E_{\mathrm{des}}) \end{aligned} \tag{4.44}$$

where E_{d} is desired level of energy for a given hop. The new Poincare map $\bar{P}(\Phi, u)$ and the sequence of points $\Phi_k \in H(\mathcal{Z})$ satisfy

$$\Phi_{k+1} = \bar{P}(\Phi_k, u_k), \quad \bar{P}(\Phi, u) : H(\mathcal{Z}) \times R \mapsto H(\mathcal{Z}) \tag{4.45}$$

with periodic point Φ^* defined as

$$\Phi^* = \bar{P}(\Phi^*, u^*) \tag{4.46}$$

For the elastic foundation, the periodic point which achieves the desired apex height is given by

$$\Phi^* = \begin{bmatrix} 0 & 0 & 0 \end{bmatrix}^T, \qquad u^* = 0 \tag{4.47}$$

We define the error state $\bar{\eta}_k$ as

$$\bar{\eta}_k = (\Phi_k - \Phi^*) = \Phi_k$$

By linearizing the Poincare map about (Φ^*, u^*), we have the approximate discrete dynamics given by

$$\begin{aligned} \bar{\eta}_{k+1} &= \bar{A}\,\bar{\eta}_k + \bar{B}u_k \\ \bar{A} &\triangleq \left.\frac{d\bar{P}(\Phi,u)}{d\Phi}\right|_{\Psi=\Psi^*,u=u^*}, \quad \bar{B} \triangleq \left.\frac{d\bar{P}(\Phi,u)}{du}\right|_{\Psi=\Psi^*,u=u^*} \end{aligned} \tag{4.48}$$

For our choice of input

$$u_k = K\bar{\eta}_k \tag{4.49}$$

the closed-loop system dynamics takes the form

$$\bar{\eta}_{k+1} = (\bar{A} + \bar{B}K)\bar{\eta}_k$$

If $\{\bar{A}, \bar{B}\}$ is controllable, we can choose K such that

$$\rho(\bar{A} + \bar{B}K) < 1 \tag{4.50}$$

and the hybrid dynamical system is asymptotically stable.

Remark 2. If the condition in (4.43) is not satisfied and the discrete controller in (4.49) is implemented, the continuous controller will have to modified. In particular, the fixed desired

value of the energy E_{des} will have to be replaced by the desired value of energy for each hop E_{d} to account for the change in the Poincare map from $P(\Psi)$ to $\bar{P}(\Phi, u)$.

4.4 Simulation Results

The mass and length parameters of the robot and the stiffness of the elastic foundation are provided below:

$$m_1 = 2.668 \text{ kg}, \quad m_2 = 0.808 \text{ kg}$$

$$\ell = 0.059 \text{ m}, \quad K_{\text{ext}} = 11560 \text{ N/m}$$

The value of r_{d} and the desired apex height were chosen as

$$r_{\text{d}} = 0.0979 \text{ m}, \qquad h_{\text{d}} = 0.2 \text{ m} \tag{4.51}$$

The parameters of the continuous controller were chosen as

$$k_e = 0.001, \qquad k_1 = 600, \qquad k_2 = 18 \tag{4.52}$$

The value of k_e was chosen to be much smaller than those of k_1 and k_2 to reduce the dominance of terms involving K_{ext}, which is $\mathcal{O}(10^4)$. The matrix A, defined in (4.42), was found to have eigenvalues: 0.0003, -0.0017 and -0.3678; the condition in (4.43) was therefore satisfied. A discrete controller was nevertheless designed and the gain matrix K in

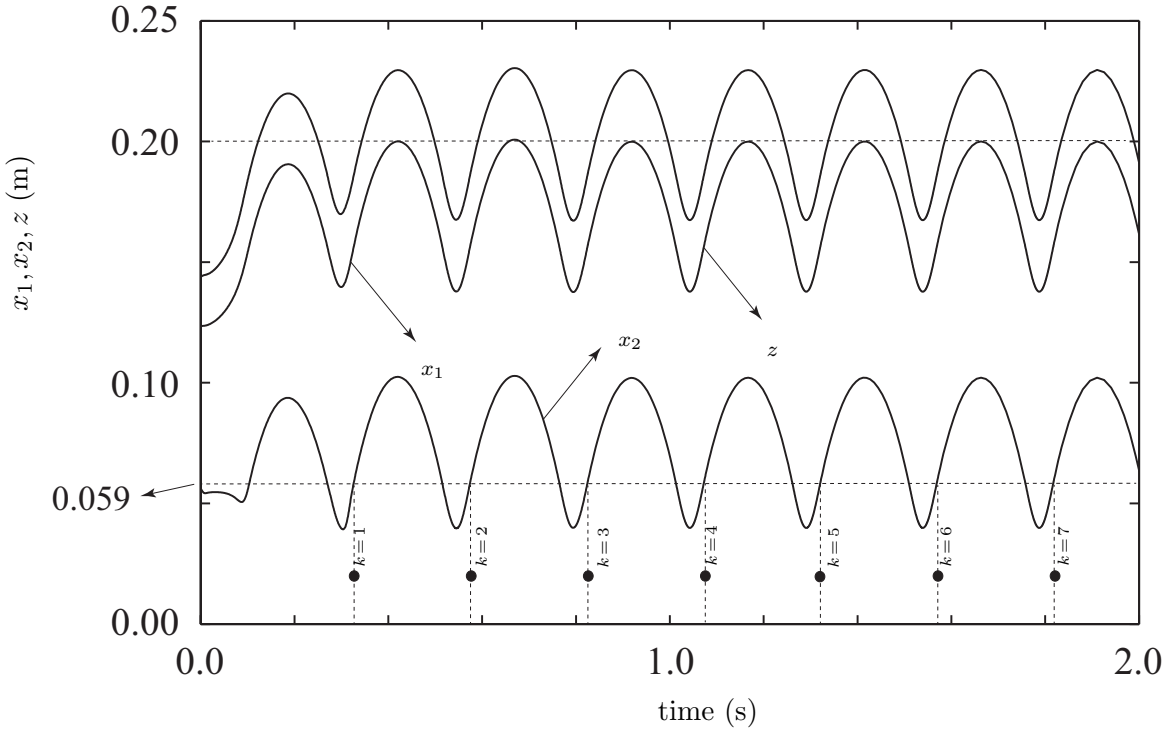

Figure 4.2: Simulation results: Plot of the height of the upper mass x_1, the lower mass x_2, and the center-of-mass z, as a function of time.

(4.49) was chosen as follows

$$K = \begin{bmatrix} 0.1000 & 0.0900 & 0.0189 \end{bmatrix} \tag{4.53}$$

This results in the closed-loop system eigenvalues: 0.0003, -0.0641 and 0.2000. The gains in (4.53) were chosen to move the eigenvalue with the largest magnitude from -0.3678 to 0.2000. The initial conditions were assumed to be

$$\begin{aligned} x_2(0) &= 0.056 \text{ m}, & y(0) &= 0.088 \text{ m} \\ \dot{x}_2(0) &= 0.0 \text{ m/s}, & \dot{y}(0) &= 0.0 \text{ m/s} \end{aligned} \tag{4.54}$$

and the results are shown in Figs.4.2 and 4.3. The displacements of the upper mass, lower

mass, and center-of-mass are plotted in Fig.4.2. The intervals of time during which $x_2 \leq \ell = 0.059$ m indicate the contact phases. The value of $x_2(0) = 0.056$ m indicates that the spring is initially compressed due to the weight of the robot. It is clear from Fig.4.2 that the apex height of the robot converges to its desired value in two hops. The discrete states Ψ are plotted in Fig.4.3; they correspond to the values of $(E - E_{\rm des})$, q_1 and q_2 at the beginning of the k-th hop, $k = 1, 2, \cdots, 7$, and they converge to zero prior to the third hop. The discrete instants of time corresponding to $k = 1, 2, \cdots, 7$ in Fig.4.3 are marked by "•" in Fig.4.2.

From the simulations we see the efficacy of the modified control method for to two mass hopping robot on an elastic foundation. We next investigate the application of the control method on elastic ground to a multi-link system. The multi-link system is chosen as a more accurate representation of a humanoid system.

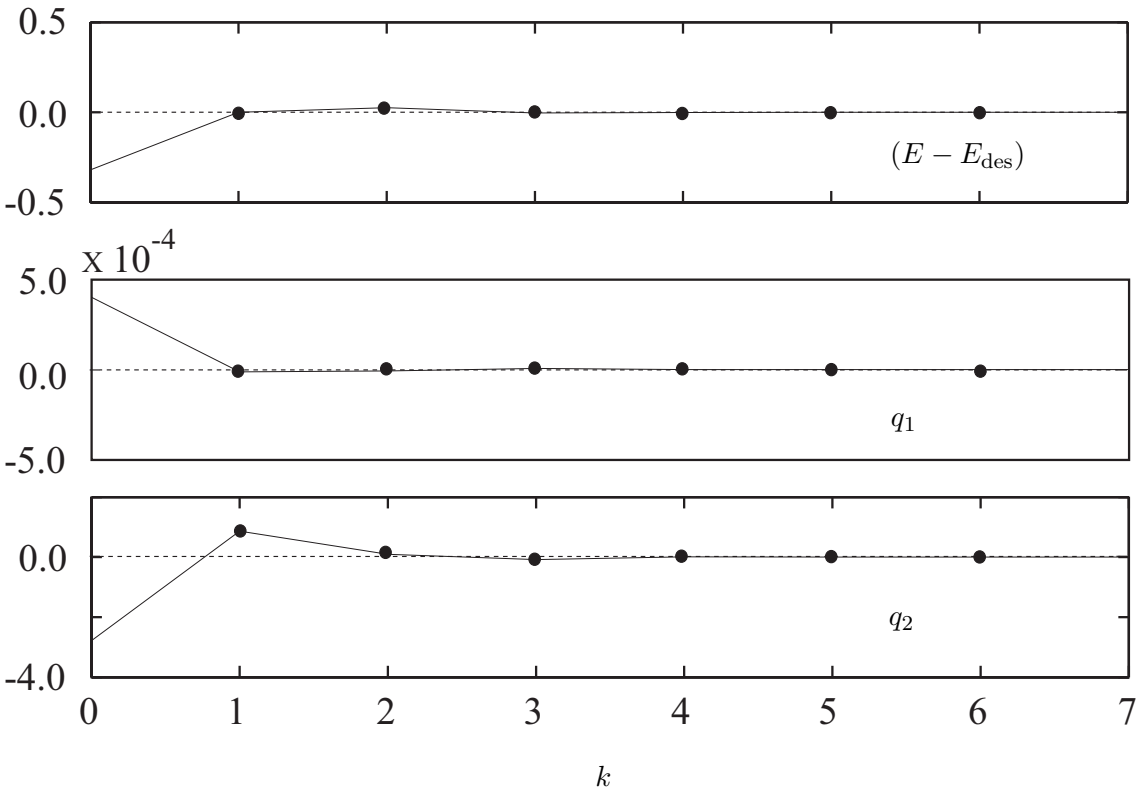

Figure 4.3: Simulation results: Errors in the discrete states $(E - E_{\rm des})$, q_1 and q_2 at the beginning of the k-th hop, $k = 1, 2, \cdots, 7$.

Chapter 5

Three-link Hopping Robot on an Elastic Foundation

From the simulation results of the two-mass hopper in Chapter 4 we see that the control method on elastic ground is capable of achieving a desired apex height for the simplified two-mass system. We now generalize the control methodology to a multi-dof linked robot system. To this end we consider the apex height control of a three-link hopping robot.

The choice of a three-linked hopping robot is such that it provides the smallest dimensional system to achieve the full control dimensions, as opposed to the four-link, which required additional objectives for the extra digrees of freedom.

The control is designed following a similar structure in Chapter 3. Additional consideration is given during both the continuous and discrete phases to account for the additional degrees-of-freedom in the system.

5.1 Dynamics

5.1.1 System Description

Consider the three-linked robot in Fig.5.1 (a), which is hopping on a massless elastic foundation of stiffness K_{ext}. It is comprised of three links of length l_1, which each have mass m_i

for $i \in 1, 2, 3$. A controllable torque is applied at the joints comprising the intersection of each link. The distance of the center-of-mass of each link is from the end of the previous link and is given by d_i. The Cartesian location of the base of the first link, point o, relative to the ground datum is given by x and y. We denote the relative angle of the ith link relative to the previous link by θ_i - see Fig.5.1. The states are defined as

$$q = \begin{bmatrix} x & y & \theta_1 & \theta_2 & \theta_3 \end{bmatrix}^T \tag{5.1}$$

The equations of motion of the hopper are given by

$$M(q)\ddot{q} + N(q, \dot{q}) = AT + F_{ext} \tag{5.2}$$

where $M(q)$ is the mass matrix; and $N(q, \dot{q})$ is the vector of Coriolis, centrifugal, and gravitational forces; and $A \in \mathbb{R}^{6\times3}$ is the matrix give below

$$A = \begin{bmatrix} 0 & 0 & 0 & 1 & 0 \\ 0 & 0 & 0 & 0 & 1 \end{bmatrix}^T, \tag{5.3}$$

T is the vector of input torques

$$T = \begin{bmatrix} \tau_1 & \tau_2 \end{bmatrix}^T, \tag{5.4}$$

and F_{ext} it the force applied by the ground on the robot given by

$$F_{ext} = \begin{bmatrix} F_x & F_y & 0 & 0 & 0 \end{bmatrix}^T \tag{5.5}$$

In Eq.(5.5), F_x and F_y denote the x and y components of the force applied to the robot by the ground at point O. The dynamics of the hopper may be separated into three phases: the flight phase for which $y > 0$; the impact phase, which occurs at the instant $y = 0$; and the contact phase, which occurs for the duration in which the foot remains in contact with the ground, $y \equiv 0$. The phases mirror those of the two-mass hopper.

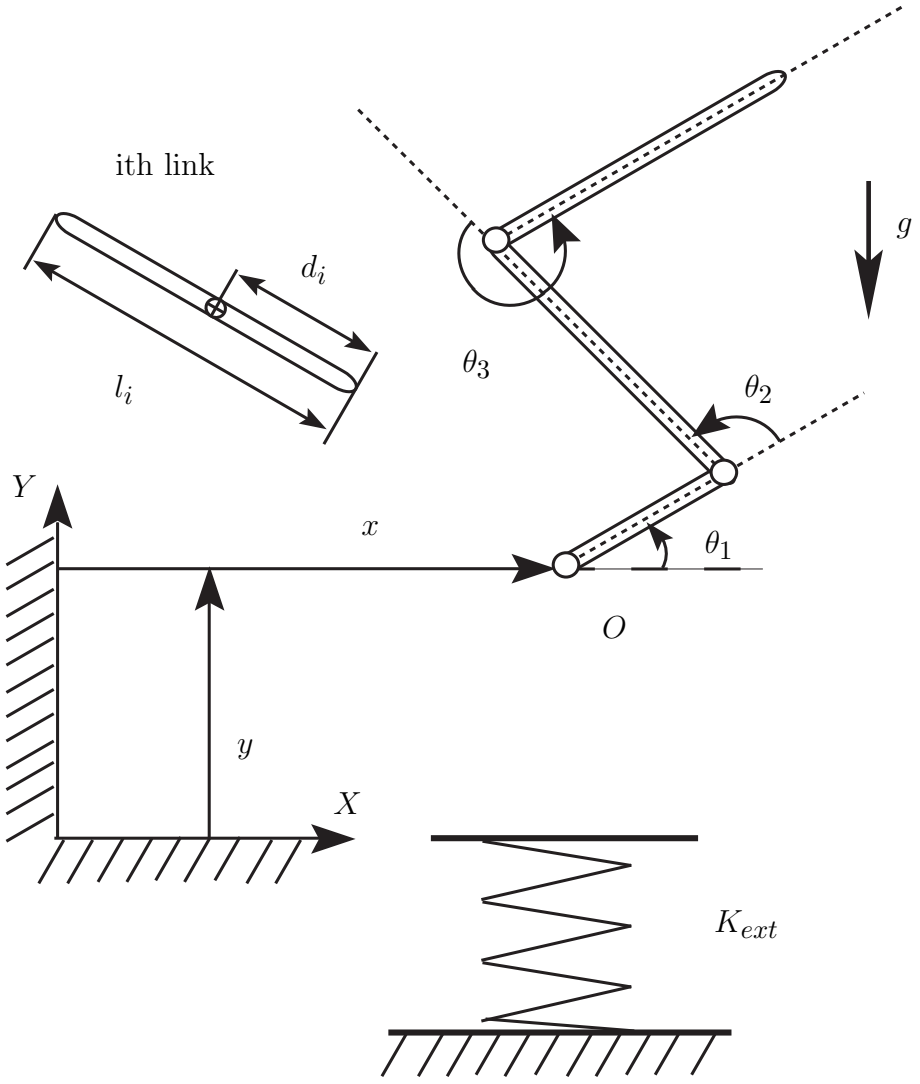

Figure 5.1: Three-link hopping robot on an elastic foundation

5.1.2 Flight Phase

During the flight phase, the following conditions hold:

$$y > 0 \qquad F_x = F_y = 0 \tag{5.6}$$

The equations of motion during the flight phase are given by

$$M(q)\ddot{q} + N(q, \dot{q}) = AT \tag{5.7}$$

where the matrix $M(q) \in \mathbb{R}^{5\times5}$ is the mass matrix and $N(q, \dot{q}) \in \mathbb{R}^5$ is the non-linear gravitational and Coriolis effects. The matrix A represents the mapping of torques to the relative states, and the vector of torques, T, it is given by

$$T = \begin{bmatrix} \tau_1, & \tau_2 \end{bmatrix}^T \tag{5.8}$$

5.1.3 Impact

At the time of impact we assume:

Assumption 1: The applied vector of torques T are not impulsive.

Assumption 1 does not imply that the vector of torques T cannot be discontinuous; it simply implies that the torques cannot produce discrete jumps in the states.

Assumption 2: The hopper's foot comes in contact with the ground only at point O.

Assumption 2 can be enforced through proper choice of control gains.

Assumption 3: At the instant the foot contacts the ground ($y = 0$), the ground applies an impulsive force that results in $\dot{x} = 0$.

Assumption 3 simply implies inelastic impact in the X direction. It can be noted that assumption 3 is not entirely physical. This is because in a physical system, the lateral force F_x is dependent on the friction force; and, thus its model or models are chosen to represent said friction. To alleviate the need of additional analysis of the model, the force is assumed to hold the point O in the x direction for the entire duration of the contact phase.

Taking the integral over the infinitesimal period of time in which the impact occurs we have

$$\int_{t_0}^{t_0+\epsilon} \ddot{q} dt = \int_{t_0}^{t_0+\epsilon} M^{-1}(q) \left[AT - N(q, \dot{q}) + F_{ext} \right] dt \tag{5.9}$$

$$\dot{q}^+ = \dot{q}^- + M^{-1}(q) F_{ext} \tag{5.10}$$

where $\dot{q}^+$ and $\dot{q}^-$ are the right and left limits in time of $\dot{q}$. This follows from our earlier work [10]. Partitioning q according to

$$q = [x \mid y \;\; \theta]^T \tag{5.11}$$

where θ is given by

$$\theta = [\theta_1 \;\; \theta_2 \;\; \theta_3]^T \tag{5.12}$$

results in the corresponding partition of $M^{-1}(q)$ given by

$$M^{-1}(q) = \left[\begin{array}{c|c} (M^{-1})_{11} & (M^{-1})_{12} \\ \hline (M^{-1})_{21} & (M^{-1})_{22} \end{array} \right] \tag{5.13}$$

Solving Eq.(5.10) results in the following change in the state variables:

$$\begin{aligned} q^+ &= q^- \\ \dot{x}^+ &= 0 \\ \begin{bmatrix} \dot{y}^+ \\ \dot{\theta}^+ \end{bmatrix} &= \begin{bmatrix} \dot{y}^- \\ \dot{\theta}^- \end{bmatrix} - (M^{-1})_{21}[(M^{-1})_{11}]^{-1}\dot{x}^- \end{aligned} \tag{5.14}$$

5.1.4 Contact Phase

For the contact phase, we make the following assumptions:

Assumption 1: The elastic foundation has no mass and behaves like a spring.

Assumption 2: Only the point O contacts the elastic surface.

Assumption 3: The vertical force exerted by the elastic foundation on the point O is non-negative, *i.e.*, $F_y \geq 0$.

Assumption 4: The horizontal force of the ground on the point O is such that it prevents motion in the X direction of point O.

During the contact phase, we may write the dynamics of the hopper which are given by

$$DM(q)D^T D\ddot{q} + DN(q,\dot{q}) = DAT + DF_{ext} \tag{5.15}$$

where D is the matrix

$$D = \begin{bmatrix} 0 & 1 & 0 & 0 & 0 \\ 0 & 0 & 1 & 0 & 0 \\ 0 & 0 & 0 & 1 & 0 \\ 0 & 0 & 0 & 0 & 1 \end{bmatrix} \tag{5.16}$$

With the external force F_y given by

$$Fy = -K_{ext}y \tag{5.17}$$

From Eqn.(5.17), the contact phase transitions to the flight phase when

$$y = 0 \qquad \dot{y} > 0 \tag{5.18}$$

Equation (5.15) during contact is identical to Eqn. (5.2), but is presented as an alternative to having to solve for F_x, or to be used for control if F_x cannot be measured.

5.1.5 Apex Height

Similar to the two-mass case, we wish to control the position of the center of mass of the hopper relative to that base of the robot, point O. To control the center of mass, we define r to be the vector from the base of the foot to the center of mass of the hopper. If r_x and r_y denote the horizontal and vertical components of r, we can write

$$r = \begin{bmatrix} r_x \\ \\ r_y \end{bmatrix} = \begin{bmatrix} f_x(q) \\ \\ f_y(q) \end{bmatrix} \tag{5.19}$$

where $f_x(q)$ and $f_y(q)$ are given by

$$\begin{aligned} f_x(q) &= a_1 \cos(\theta_1) + a_2 \cos(\theta_1 + \theta_2) + \\ & \quad a_3 \cos(\theta_1 + \theta_2 + \theta_3) \end{aligned} \tag{5.20}$$

$$
\begin{aligned}
f_y(q) &= a_1 \sin(\theta_1) + a_2 \sin(\theta_1 + \theta_2) + \\
& \quad a_3 \sin(\theta_1 + \theta_2 + \theta_3)
\end{aligned} \tag{5.21}
$$

in Eq.(5.20) and (5.21), the constants have the expressions

$$
\begin{aligned}
a_1 &= \frac{m_1 d_1 + (m_2 + m_3) l_1}{\overline{m}} \\
a_2 &= \frac{m_2 d_2 + m_3 l_2}{\overline{m}} \\
a_3 &= \frac{m_3 d_3}{\overline{m}} \\
\overline{m} &= m_1 + m_2 + m_3
\end{aligned} \tag{5.22}
$$

If z denotes the height of the center-of-mass of the hopping robot, we have

$$
z = y + r_y \tag{5.23}
$$

For each flight phase, the apex height is defined as the maximum value of z, and is denoted by h.

Differentiating r with respect to time gives

$$
\dot{r} = \begin{bmatrix} \dot{r}_x \\ \\ \dot{r}_y \end{bmatrix} = \begin{bmatrix} J_x(q) \\ \\ J_y(q) \end{bmatrix} \dot{q} \tag{5.24}
$$

where $J_x(q)$ and $J_y(q)$ are Jacobian matrices.

From the equations of motion in Eqn.(5.2) we find that dynamics of z may be given by

$$
\overline{m}\ddot{z} = -\overline{m}g + F_y \tag{5.25}
$$

5.2 Hybrid Control Strategy

5.2.1 Feedback Linearization

The control of the three-link, hopping robot is defined based on the relative center of mass, given by r in Eqn. (5.19). To do this, we define the error states e to be given by

$$e = \begin{bmatrix} e_x \\ \\ e_y \end{bmatrix} = r - r_{\mathrm{d}} = \begin{bmatrix} r_x - r_{\mathrm{d,x}} \\ \\ r_y - r_{\mathrm{d,y}} \end{bmatrix} \tag{5.26}$$

where $r_{\mathrm{d,x}} = 0$ and $r_{\mathrm{d,y}}$ s a constant defined based as the desired resting height of the center of mass relative to the base o. Differentiating Eqn. (5.26) and substituting Eqn. (5.24) gives

$$\dot{e} = J(q)\dot{q} = \begin{bmatrix} J_x(q) \\ \\ J_y(q) \end{bmatrix} \dot{q} \tag{5.27}$$

Differentiating a second time we find the dynamics of e to be given by

$$\ddot{e} = J(q)\ddot{q} + \dot{J}(q)\dot{q} \tag{5.28}$$

Substituting Eqn. (5.2) into Eqn. (5.28) gives

$$\ddot{e} = J(q)M^{-1}(q)\left[AT + F_{ext} - N(q,\dot{q})\right] + \dot{J}(q)\dot{q} \tag{5.29}$$

Defining the vector of torques T to be given by

$$T = \left[J(q)M^{-1}(q)\right]^{\#} \left\{v_g + J(q)M^{-1}(q)[N(q,\dot{q}) - F_{ext}] - \dot{J}\dot{q}\right\} \tag{5.30}$$

where $(\cdot)^{\#}$ is the right pseudo-inverse of $(\cdot)$, results in

$$\ddot{e} = \begin{bmatrix} e_x \\ \\ e_y \end{bmatrix} = v_g = \begin{bmatrix} v_x \\ \\ v_y \end{bmatrix} \tag{5.31}$$

5.2.2 Controller Design in X Direction

For the control of the system in the X we see that we desire to have $e_x \to 0$, which will prevent any lateral motion. We further see that when $e_x \equiv 0$ that the impulse dynamics given in Eqn.(5.14) result in an impulse of magnitude 0 as there is no linear momentum to cancel at the time of impact. Designing v_x to be given by

$$v_x = -K_x e_x - K_{d,x} \dot{e}_x \tag{5.32}$$

where K_x and $K_{d,x}$ are positive constants, results in asymptotic convergence of $e \to 0$ during the continuous phases.

5.2.3 Control Problem Definition for Y Direction

It can be verified that, as with the two-mass system, $e \equiv 0 \to \dot{e} \equiv 0$, which implies no relative motion of the center of mass.

If there is no relative motion of the center of mass, the total energy of the system is the sum of the kinetic and potential energies of the center-of-mass plus the potential energy stored in the elastic foundation. The potential energy of the center-of-mass is defined relative to the datum $z = z_{\mathrm{d}}$, where

$$z_{\mathrm{d}} \triangleq z \mid_{(r_Y = r_{\mathrm{d,y}})} = r_{\mathrm{d,y}}$$

In the absence of relative motion of the center of mass, the total energy can be written as

$$E = \overline{m}\left[\frac{1}{2}\dot{z}^2 + g(z - z_{\mathrm{d}})\right] + \frac{1}{2}\lambda K_{\mathrm{ext}}\,(z - z_{\mathrm{d}})^2 \tag{5.33}$$

where

$$\lambda = \begin{cases} 0 \quad : \quad y \geq \ell - \text{Flight Phase} \\ 1 \quad : \quad y < \ell - \text{Contact Phase} \end{cases} \tag{5.34}$$

The second term on the right-hand side of (5.33) represents the potential energy stored in the spring when the two masses are in their nominal position relative to one another. For the robot to reach its desired apex height h_{d}, the total energy should be equal to

$$E \equiv E_{\mathrm{des}} = \overline{m}\, g(h_{\mathrm{d}} - z_{\mathrm{d}}) \tag{5.35}$$

in addition to $e \equiv 0$. The desired equilibrium configuration is therefore given by

$$(E - E_{\mathrm{des}}, e, \dot{e}) = (0, 0, 0) \tag{5.36}$$

5.2.4 Continuous Controller Design for Y Direction, Backstepping

For the controller design in the Y direction we will assume that $e_x \equiv 0$. This is a fair assumption as the convergence of the dynamics in the X direction are independent of the control in the Y direction. With the objective of stabilizing the equilibrium in Eq. (5.36),

we first define the Lyapunov function candidate

$$V_1 = \frac{1}{2} k_e \left(E - E_{\text{des}}\right)^2 \tag{5.37}$$

where k_e is a positive constant. It should be noted that V_1 is a function of λ (since E is a function of λ), but it is continuously differentiable in both the flight phase and contact phase. The Lyapunov function candidates introduced below can be used for our analysis of stability in both phases; and, therefore, we treat λ as constant and do not make any distinction between the two phases in our derivation. Using Eqs.(5.26), (5.25), (5.33), and (5.37), $\dot{V}_1$ can be computed as

$$\begin{aligned}
\dot{V}_1 &= k_e \left(E - E_{\text{des}}\right) \dot{E} \\
&= k_e \left(E - E_{\text{des}}\right) \dot{z} \left[\overline{m}(\ddot{z} + g) + \lambda K_{\text{ext}}(z - z_{\text{d}})\right] \\
&= k_e \left(E - E_{\text{des}}\right) \lambda K_{\text{ext}} \dot{z} e_y
\end{aligned} \tag{5.38}$$

By choosing

$$e = \left\{-\lambda k_e \left(E - E_{\text{des}}\right) \dot{z}\right\} \triangleq \phi_1 \tag{5.39}$$

we can make $\dot{V}_1$ negative semi-definite; therefore, integrator backstepping is introduced by defining the new variable

$$\zeta_1 = e + \lambda k_e \left(E - E_{\text{des}}\right) \dot{z} = (e - \phi_1) \tag{5.40}$$

and the composite Lyapunov function

$$V_2 = V_1 + \frac{1}{2}q_1^2 = \frac{1}{2}k_e\left(E - E_{\text{des}}\right)^2 + \frac{1}{2}\zeta_1^2 \tag{5.41}$$

where where k_1 is a positive constant. Differentiating V_2 and substituting Eq.(5.38) and Eq.(5.40), we get

$$\begin{aligned}
\dot{V}_2 &= k_e\left(E - E_{\text{des}}\right)\lambda K_{\text{ext}}\dot{z}e_y + \zeta_1\dot{\zeta}_1 \\
&= k_e\left(E - E_{\text{des}}\right)\lambda K_{\text{ext}}\dot{z}\left[\zeta_1 - \lambda k_e\left(E - E_{\text{des}}\right)\dot{z}\right] + \zeta_1\dot{\zeta}_1 \\
&= -\lambda^2 k_e^2 K_{\text{ext}}\left(E - E_{\text{des}}\right)^2\dot{z}^2 \\
&\qquad + \zeta_1\left[\dot{\zeta}_1 + k_e\left(E - E_{\text{des}}\right)\lambda K_{\text{ext}}\dot{z}\right]
\end{aligned} \tag{5.42}$$

By choosing $k_1 > 0$ and

$$\dot{\zeta}_1 = \left\{-\lambda k_e K_{\text{ext}}\left(E - E_{\text{des}}\right)\dot{z} - k_1\zeta_1\right\} \triangleq \phi_2 \tag{5.43}$$

we can make $\dot{V}_2$ negative semi-definite. We introduce integrator backstepping again by defining the new variable

$$\zeta_2 = (\dot{\zeta}_1 - \phi_2) \tag{5.44}$$

and the composite Lyapunov function

$$\begin{aligned}
V_3 &= V_2 + \frac{1}{2}\zeta_2^2 \\
&= \frac{1}{2}k_e\left(E - E_{\text{des}}\right)^2 + \frac{1}{2}\zeta_1^2 + \frac{1}{2}\zeta_2^2
\end{aligned} \tag{5.45}$$

Differentiating V_3 and substituting Eq.(5.42) and Eq.(5.44), we get

$$\begin{aligned}
\dot{V}_3 &= -\lambda^2 k_e^2 K_{\text{ext}} \left(E - E_{\text{des}}\right)^2 \dot{z}^2 \\
&\quad + \zeta_1 \left[\dot{\zeta}_1 + \lambda k_e K_{\text{ext}} \left(E - E_{\text{des}}\right) \dot{z}\right] + \zeta_2 \dot{\zeta}_2 \\
&= -\lambda^2 k_e^2 K_{\text{ext}} \left(E - E_{\text{des}}\right)^2 \dot{z}^2 \\
&\quad + \zeta_1 \left[\dot{\zeta}_1 - \phi_2 - k_1 \zeta_1\right] + (\dot{\zeta}_1 - \phi_2)(\ddot{\zeta}_1 - \dot{\phi}_2) \\
&= -\lambda^2 k_e^2 K_{\text{ext}} \left(E - E_{\text{des}}\right)^2 \dot{z}^2 - k_1 \zeta_1^2 \\
&\quad + \zeta_2 \left[\ddot{\zeta}_1 - \dot{\phi}_2 + \zeta_1\right]
\end{aligned} \tag{5.46}$$

Our choice of

$$\ddot{\zeta}_1 = \dot{\phi}_2 - \zeta_1 - k_2 \zeta_2, \qquad k_2 > 0 \tag{5.47}$$

results in a negative semi-definite $\dot{V}_3$ and yields the controller

$$v_y = \ddot{\phi}_1 + \dot{\phi}_2 - \zeta_1 - k_2 \zeta_2 \tag{5.48}$$

The above equation was obtained from Eq.(5.47) by substituting Eqs.(5.31) and (5.40). From the definition of ϕ_1 in Eq.(5.39), it is clear that $\ddot{\phi}_1$ will involve the third derivative of z. This is not a problem since the third derivative of z can be computed easily from Eq.(5.25) as

$$\dddot{z} = -\lambda \frac{1}{m} K_{\text{ext}} \dot{y} \tag{5.49}$$

The complete control law is given by Eqs.(5.48), (5.32), (5.31), and (5.30).

5.2.5 Stability Analysis

Assuming $e_x \equiv 0$, and using Eqs.(5.19), (5.23), (5.33), (5.25), (5.40) and (5.44) it can be shown that

$$(E - E_{\text{des}}, e_y, \dot{e}_y) = (0, 0, 0) \;\Leftrightarrow\; (E - E_{\text{des}}, \zeta_1, \zeta_2) = (0, 0, 0)$$

Therefore, V_3 in Eq.(5.45) is a candidate Lyapunov function for investigating the stability of the equilibrium in Eq.(5.36).

In the flight phase, $\lambda = 0$. For the control law, given by Eq.(5.48), the derivative of the Lyapunov function in Eq.(5.46) can be shown to be

$$\dot{V}_3 = -k_1\zeta_1^2 - k_2\zeta_2^2 \leq 0 \tag{5.50}$$

Therefore, $(E - E_{\text{des}}, \zeta_1, \zeta_2) = (0, 0, 0)$ is stable.

In the contact phase, $\lambda = 1$. For the control law given by Eq.(5.48), the derivative of the Lyapunov function in Eq.(5.46) is

$$\dot{V}_3 = -k_e K_{\text{ext}} \left(E - E_{\text{des}}\right)^2 \dot{z}^2 - k_1\zeta_1^2 - k_2\zeta_2^2 \leq 0 \tag{5.51}$$

Therefore, $(E - E_{\text{des}}, \zeta_1, \zeta_2) = (0, 0, 0)$ is stable.

Remark 3. The stability of $(E - E_{\text{des}}, \zeta_1, \zeta_2) = (0, 0, 0)$ in the flight and contact phases does not guarantee its stability for the hybrid dynamics.

5.2.6 Discrete Controller for Stabilization of Hybrid Dynamics

To investigate the stability of the hybrid dynamic system, we use a Poincare map with the Poincare section defined by the instant when the system transitions from the contact phase to the flight phase. The Poincare section is defined as

$$\begin{aligned} \mathcal{Z} &\coloneqq \Big\{ X \in \mathbb{R}^8 |\ y = 0,\ \dot{y} > 0,\ \dot{x} = 0 \Big\} \\ \Rightarrow\ \mathcal{Z} &\coloneqq \Big\{ X \in \mathbb{R}^8 |\ z = e_y + z_d,\ \dot{z} > \dot{e}_y,\ \dot{x} = 0 \Big\} \end{aligned} \tag{5.52}$$

where X is defined as

$$X = \begin{bmatrix} x & \dot{z} & \theta_1 & \dot{\theta}_1 & \theta_2 & \dot{\theta}_2 & \theta_3 & \dot{\theta}_3 \end{bmatrix}^T$$

From the system dynamics, we can find that the Poincare map may be considered independent of the variable x as it only places a translation on the initial conditions of the section without effecting the dynamics. We therefore define the Poincare section using the coordinates Ψ, where Ψ is defined by the reduced coordinates

$$\Psi = \begin{bmatrix} \dot{z} & \theta_1 & \dot{\theta}_1 & \theta_2 & \dot{\theta}_2 & \theta_3 & \dot{\theta}_3 \end{bmatrix}^T \tag{5.53}$$

Defining the reduced section $\mathcal{L}$ as

$$\mathcal{L} \coloneqq \Big\{ X \in \mathbb{R}^7 |\ y = 0,\ \dot{y} > 0,\ \dot{x} = 0 \Big\} \subset \mathcal{Z} \tag{5.54}$$

The Poincare map $P(\Psi)$ and the sequence of points $\Psi_k \in \mathcal{L}$ satisfy

$$\Psi_{k+1} = P(\Psi_k) \tag{5.55}$$

with periodic point Ψ^* defined as

$$\Psi^* = P(\Psi^*) \tag{5.56}$$

For the elastic foundation, the periodic points of interest satisfy

$$\Psi^* \in \{X \in \mathcal{L} \mid E = E_{des},\ e = 0,\ \dot{e} = 0\} \tag{5.57}$$

We define the error state η_k as

$$\eta_k = (\Psi_k - \Psi^*)$$

By linearizing the Poincare map about Ψ^*, we have the approximate discrete dynamics given by

$$\eta_{k+1} = A\,\eta_k \qquad A \triangleq \left.\frac{dP(\Psi)}{d\Psi}\right|_{\Psi=\Psi^*} \tag{5.58}$$

The periodic point will be asymptotically stable if and only if

$$\rho(A) < 1 \tag{5.59}$$

where $\rho(A)$ is the spectral radius of A. Since the condition in Eq.(5.59) may not be satisfied, we design a discrete controller to stabilize the closed-loop system; the discrete controller is discussed next.

To design the discrete controller, we define the additional state E_d as the desired energy

input to backstepping controller. To this end we define the discrete input $u(k)$ to be given by

$$u(k) \triangleq (E_{\mathrm{d}} - E_{\mathrm{des}}) \tag{5.60}$$

We see that at the periodic point Ψ^*, that

$$u(k) = u^* = 0 \tag{5.61}$$

The new Poincare map $\bar{P}(\Psi, u)$ satisfies

$$\Psi_{k+1} = \bar{P}(\Psi_k, u_k) \tag{5.62}$$

with periodic point Φ^* defined as

$$\Psi^* = \bar{P}(\Psi^*, u^*) = \bar{P}(\Psi^*, 0) \tag{5.63}$$

We define the error state $\bar{\eta}_k$ as

$$\bar{\eta}_k = (\Psi_k - \Psi^*)$$

and linearizing the Poincare map about (Φ^*, u^*), we have the approximate discrete dynamics given by

$$\begin{aligned} &\bar{\eta}_{k+1} = \bar{A}\,\bar{\eta}_k + \bar{B}u_k \\ &\bar{A} \triangleq \left.\frac{d\bar{P}(\Phi, u)}{d\Phi}\right|_{\Psi=\Psi^*, u=u^*}, \quad \bar{B} \triangleq \left.\frac{d\bar{P}(\Phi, u)}{du}\right|_{\Psi=\Psi^*, u=u^*} \end{aligned} \tag{5.64}$$

For our choice of input

$$u_k = K\bar{\eta}_k \tag{5.65}$$

the closed-loop system dynamics takes the form

$$\bar{\eta}_{k+1} = (\bar{A} + \bar{B}K)\bar{\eta}_k$$

If $\{\bar{A}, \bar{B}\}$ is controllable, we can choose K such that

$$\rho(\bar{A} + \bar{B}K) < 1 \tag{5.66}$$

and the hybrid dynamical system is asymptotically stable.

Remark 4. If the condition in Eq.(5.59) is not satisfied and the discrete controller in Eq.(5.65) is implemented, the continuous controller will have to be modified. In particular, the fixed desired value of the energy E_{des} will have to be replaced by the desired value of energy for each hop E_{d} to account for the change in the Poincare map from $P(\Psi)$ to $\bar{P}(\Phi, u)$.

5.3 Simulation Results

For the three-link hopper, the masses are assumed to be

$$m_1 = 2\ kg,\ m_2 = 2\ kg,\ m_3 = 2\ kg \tag{5.67}$$

The length of the links of the hopper are assumed to be

$$l_1 = l_2 = l_3 = 0.3\ m \tag{5.68}$$

and the distance to the center of mass of each link - see Fig.3.1 are assumed to be

$$d_1 = d_2 = d_3 = 0.15\ m \tag{5.69}$$

The moment of inertia of each link is computed as

$$I_i = \frac{1}{12} m_i l_i^2 \qquad \forall i \in [1, 4] \tag{5.70}$$

The gains used for the continuous control are

$$\begin{aligned} &K_x = 8000 \quad K_{d,x} = 300 \quad k_e = 0.01 \quad k_1 = 300 \\ &k_2 = 10 \end{aligned} \tag{5.71}$$

and the set point y_d for the continuous control is

$$y_d = 0.38\ m \tag{5.72}$$

We choose the desired apex height of the center of mass to be 0.65 meters and compute

the periodic point, (χ^*, ν^*) to be given by

$$\begin{array}{lll} \chi_1^* = 0.0547 & \chi_2^* = 0.0 & \chi_3^* = -0.4361 \\ \chi_4^* = 0.0 & \chi_5^* = 1.6828 & \chi_6^* = 0.0 \\ E_d^* = 1.5892 & & \end{array} \tag{5.73}$$

with all values given in rad and rad/s where appropriate. The stabilizing control gains K for the periodic point in Eq.(5.65) are by solved by usng the discrete LQR problem

$$\begin{array}{lll} K_1 = 0.1 & K_2 = -0.03 & K_3 = 0.1 \\ K_4 = -0.04 & K_5 = -0.1 & K_6 = 0.003 \end{array} \tag{5.74}$$

We choose the initial configuration of the system is assumed to be

$$\begin{aligned} (x(0), \dot{x}(0), y(0), \dot{y}(0)) &= (0.00, 0.00, 0.05, 0.00) \\ \theta(0) &= [0.2041,\ -0.6979,\ 1.1537]^T \\ \dot{\theta}(0) &= [0.00,\ 0.00,\ 0.00] \end{aligned} \tag{5.75}$$

where the units are in meters, rad, and rad/sec. These initial conditions were chosen such that the center of mass of the hopper lies vertically above the point of support. The initial value of the discrete control input is chosen to be

$$u(0) = 0 \Rightarrow E_d(0) = E_d^* \tag{5.76}$$

Figure 5.2 shows the height of the center of mass as a function of time. It can be seen that the center of mass converges to the desired height in approximately 4 hops. Figure 5.3

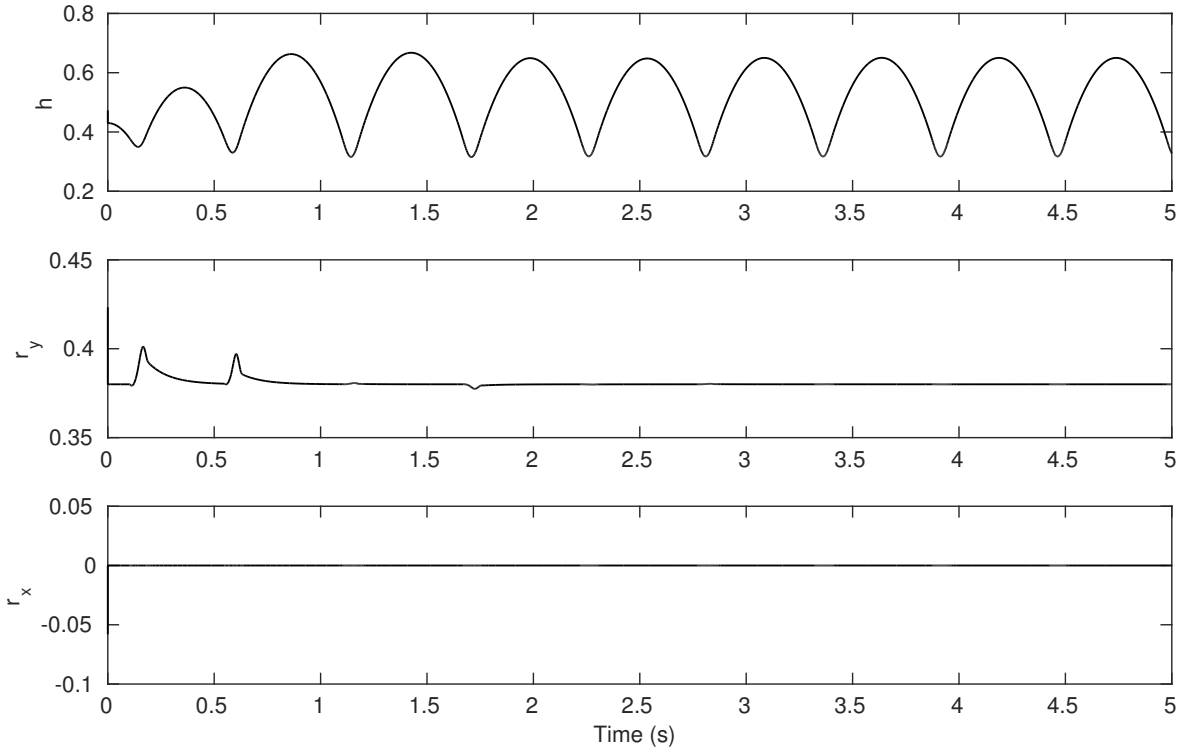

Figure 5.2: Center of mass height and relative center of mass for the three-link hopper

displays the input torques τ_1, τ_2, and τ_3. The sharp peaks indicate the discontinuous jumps in the torques immediately following impact.

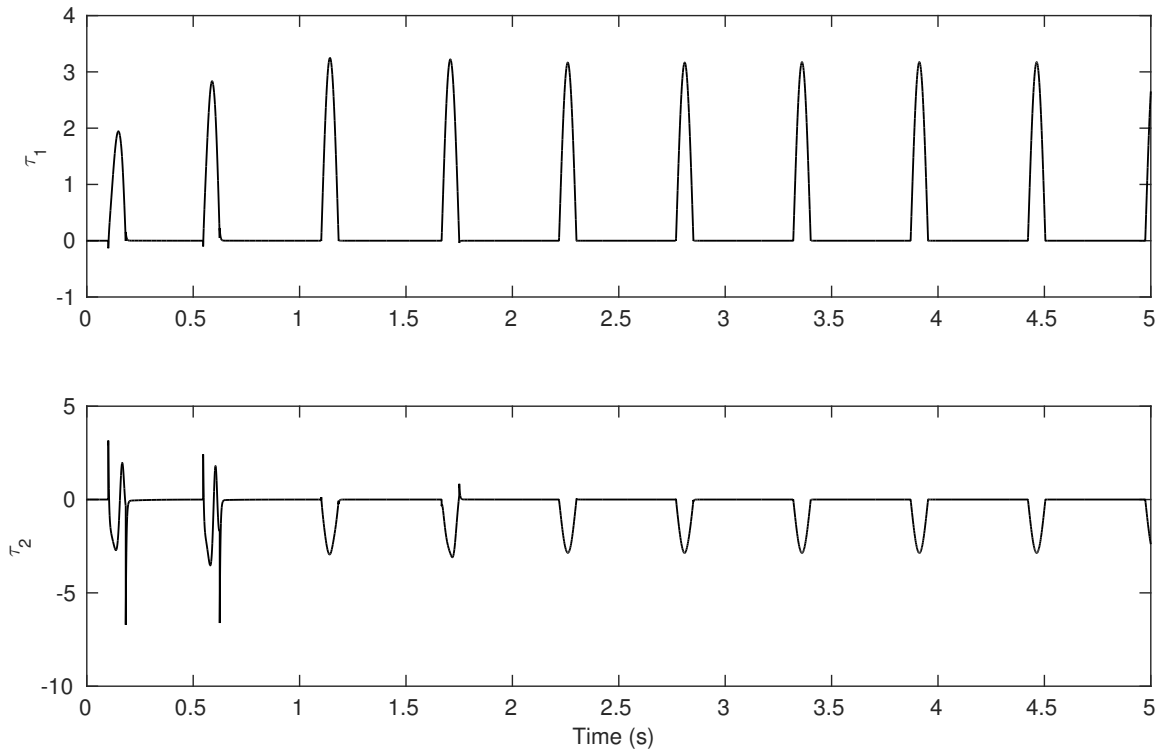

Figure 5.3: Input torques for the three-link hopper

Chapter 6

Conclusions

Presented first was a method of controlling a two-mass hopping robot interacting with rigid ground. The contact between the lower mass and the ground was considered to be inelastic which results in an impulsive reaction when the mass contacts the rigid ground. The control utilizes feedback linearization to stabilize the system during continuous motion. A discrete feedback controller on the control parameters provides stability to a desired apex height. Efficacy of the control method is initially shown through simulation. Then the robustness and applicability are tested through experiments. The experiments utilize a voice coil linear actuator to provide the force between the two-masses and a linear guide to measure the distance between the masses as well as the height. From the experiments, we saw the convergence of the algorithm, although the maximum height was restricted by the maximum force able to be applied by the voice coil.

From the control results of the two-mass hopper on rigid ground, a control method for a four-link hopping robot interacting with rigid ground it presented. Following the strategy of the two-mass hopper, feedback linearization is used in continuous time to stabilize the four-link hopper. Discrete variations of a control parameter are then used to ensure asymptotic stability to a desired apex height. Simulation results are then presented to show the efficacy of the control algorithm.

Following the control of the four-link hopper, investigation of the control method on an elastic foundation was conducted. Through a simple investigation with a two-mass,

hopping robot, it was shown that modification of the control method used when interacting with rigid ground was required. To this end, a modified control method was proposed. The control method utilized backstepping to produce a continuous stabilizing controller. Discrete variations of the control parameters were used with each hop to stabilize the system to a desired apex height. Simulation results are presented to show the efficacy of the control method.

From the control of a two-mass robot on elastic ground, the control method is extended for the control of a three-link hopper interacting with elastic ground. The control method uses backstepping for continuous stabilization. Then a discrete variation of a control parameter is used to stabilize the system to a desired apex height. The control method is verified through simulation results.

From this thesis we see the use of chaos control in the use of a hybrid dynamic system to achieve period orbits. The control relies on the construction of continuous controllers to ensure internal stability during the continuous portion of the orbit, and the discrete chaos controller provides stability of the whole of the orbit. Alternate methods were presented here for different hopping robots with different surface interactions.

Further works include investigation of a system with lateral motion, as well as system with multiple legs.

BIBLIOGRAPHY

BIBLIOGRAPHY

[1] Linear Voice Coil Motor Actuator, Model LCVM-051-165-01. www.moticont.com/lvcm-051-165-01.htm. accessed 20-Nov-2014.

[2] Servo drives - brushed, analog, panel mount, Model 25A8. www.a-m-c.com. accessed 20-Nov-2014.

[3] Single-board real-time hardware, Model DS1104. www.dspace.com. accessed 20-Nov-2014.

[4] Transmissive optical encoder module, Model EM1-0-120-N. www.usdigital.com/products/encoders/incremental/modules/EM1. accessed 20-Nov-2014.

[5] R Alexander. Three uses for springs in legged locomotion. *The International Journal of Robotics Research*, 9(2):53–61, 1990.

[6] R. Altendorfer, D.E Koditschek, and P. Holmes. Towards a factored analysis of legged locomotion models. In *IEEE International Conference on Robotics and Automation*, volume 1, pages 37–44. IEEE, 2003.

[7] R. Altendorfer, D.E Koditschek, and P. Holmes. Stability analysis of legged locomotion models by symmetry-factored return maps. *The International Journal of Robotics Research*, 23(10-11):979–999, 2004.

[8] R. Blickhan. The spring-mass model for running and hopping. *Journal of biomechanics*, 22(11):1217–1227, 1989.

[9] N. Boccara. *Modeling complex systems*. Springer Verlag, 2004.

[10] Louis L Flynn, Rouhollah Jafari, and Ranjan Mukherjee. Active synthetic-wheel biped with torso. *IEEE Transactions on Robotics*, 26(5):816–826, 2010.

[11] RM Ghigliazza, R. Altendorfer, P. Holmes, and D. Koditschek. A simply stabilized running model. *SIAM review*, 2:519–549, 2005.

[12] RM Ghigliazza, Richard Altendorfer, Philip Holmes, and D Koditschek. A simply stabilized running model. *SIAM Journal on Applied Dynamical Systems*, 2(2):187–218, 2003.

[13] K.A. Hamed and JW Grizzle. Robust event-based stabilization of periodic orbits for hybrid systems: Application to an underactuated 3d bipedal robot. In *Proceedings of the 2013 American Control Conference*, 2013.

[14] J.K. Hodgins and MN Raibert. Adjusting step length for rough terrain locomotion. *Robotics and Automation, IEEE Transactions on*, 7(3):289–298, 1991.

[15] P. Holmes, R.J. Full, D. Koditschek, and J. Guckenheimer. The dynamics of legged locomotion: Models, analyses, and challenges. *Siam Review*, 48:207–304, 2006.

[16] SH Hyon, T. Emura, and T. Mita. Dynamics-based control of a one-legged hopping robot. *Proceedings of the Institution of Mechanical Engineers, Part I: Journal of Systems and Control Engineering*, 217(2):83–98, 2003.

[17] M. Ishikawa, A. Neki, J.I. Imura, and S. Hara. Energy preserving control of a hopping robot based on hybrid port-controlled Hamiltonian modeling. In *Control Applications, 2003. CCA 2003. Proceedings of 2003 IEEE Conference on*, volume 2, pages 1136–1141. IEEE, 2003.

[18] S. Kajita, T. Nagasaki, K. Kaneko, K. Yokoi, and K. Tanie. A hop towards running humanoid biped. In *Robotics and Automation, 2004. Proceedings. ICRA'04. 2004 IEEE International Conference on*, volume 1, pages 629–635. IEEE, 2004.

[19] H. K. Khalil. *Nonlinear Systems*. Prentice Hall, 3rd edition, 2002.

[20] HK Khalil. *Nonlinear Systems*. Prentice Hall, New Jersey, 2002.

[21] Frank B Mathis and Ranjan Mukherjee. Apex height control of a two-mass hopping robot. In *Proc. 2013 IEEE International Conference on Robotics and Automation (ICRA)*, pages 4785–4790, Karlsruhe, Germany, 2013.

[22] Frank B Mathis and Ranjan Mukherjee. Apex height control of a two-mass robot hopping on a rigid foundation. *Mechanism and Machine Theory*, 105:44–57, 2016.

[23] Frank B Mathis and Ranjan Mukherjee. Two-mass robot hopping on an elastic foundation: Apex height control. In *2016 IEEE First International Conference on Control, Measurement and Instrumentation (CMI)*, pages 167–171. IEEE, 2016.

[24] I. Poulakakis and JW Grizzle. Formal embedding of the spring loaded inverted pendulum in an asymmetric hopper. In *Proceedings of the European Control Conference*, 2007.

[25] I. Poulakakis and J.W. Grizzle. The spring loaded inverted pendulum as the hybrid zero dynamics of an asymmetric hopper. *Automatic Control, IEEE Transactions on*, 54(8):1779–1793, 2009.

[26] M.H. Raibert. *Legged Robots that Balance*. The MIT Press, Cambridge, MA, 1985.

[27] Y. Saitou, T. Nagano, T. Seki, M. Ishikawa, and S. Hara. Optimal high-jump control of linear 1-dof trampoline robot. In *SICE 2002. Proceedings of the 41st SICE Annual Conference*, volume 4, pages 2527–2530. IEEE, 2002.

[28] U. Saranli, W.J. Schwind, and D.E. Koditschek. Toward the control of a multi-jointed, monoped runner. In *Robotics and Automation, 1998. Proceedings. 1998 IEEE International Conference on*, volume 3, pages 2676–2682. IEEE, 1998.

[29] E. Scholl and H.G. Schuster. *Handbook of chaos control*. Wiley-VCH, Weinheim, 2008.

[30] W.J. Schwind and D.E. Koditschek. Control of forward velocity for a simplified planar hopping robot. In *Robotics and Automation, 1995. Proceedings., 1995 IEEE International Conference on*, volume 1, pages 691–696. IEEE, 1995.

[31] J.E Seipel and P. Holmes. Running in three dimensions: Analysis of a point-mass sprung-leg model. *The International Journal of Robotics Research*, 24(8):657–674, 2005.

[32] J.E. Seipel and P. Holmes. Three-dimensional translational dynamics and stability of multi-legged runners. *The International Journal of Robotics Research*, 25(9):889–902, 2006.